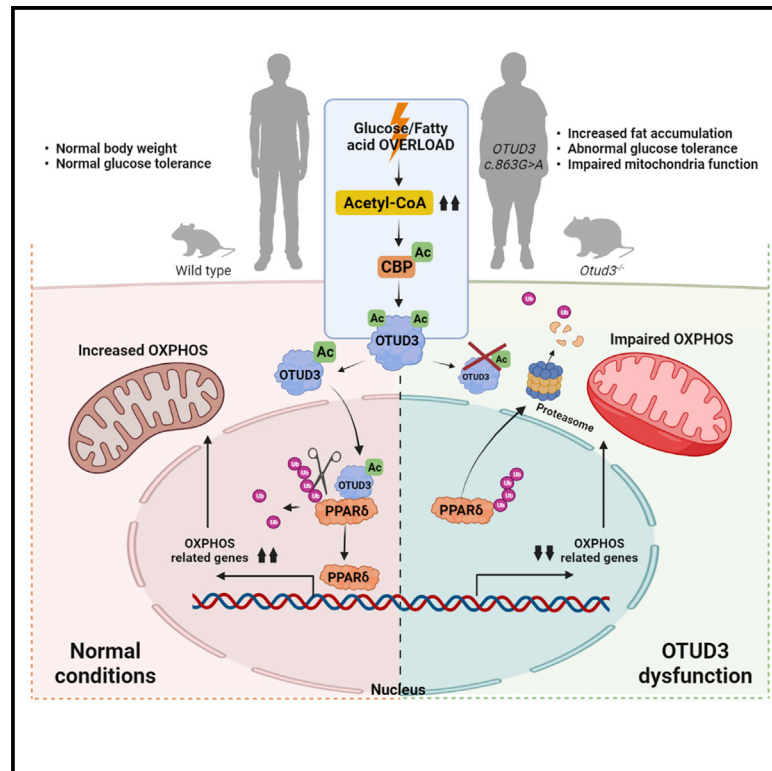


# Cell Metabolism

## Deubiquitinase OTUD3 regulates metabolism homeostasis in response to nutritional stresses

### Graphical abstract



### Authors

Na Zhou, Hailong Qi, Junjun Liu, ..., Yan Jin, Yongfeng Song, Yuxin Yin

### Correspondence

syf198506@163.com (Y.S.), yinyuxin@bjmu.edu.cn (Y.Y.)

### In brief

Zhou et al. report a new metabolic-syndrome-associated mutation in the *OTUD3* deubiquitinase found in a MODY-like family. They discover that glucose and fatty acids can trigger translocation of OTUD3 to the nucleus, where it regulates energy metabolism by stabilizing PPAR $\delta$ .

### Highlights

- *OTUD3* c.863G>A in humans is associated with obesity and a higher risk of diabetes
- OTUD3 regulates energy metabolism by blocking ubiquitin-dependent PPAR $\delta$  degradation
- Glucose and fatty acids evoke OTUD3 nuclear translocation by CBP-dependent acetylation
- CBP-OTUD3 signaling pathway may be a novel regulatory mechanism for energy metabolism

Article

# Deubiquitinase OTUD3 regulates metabolism homeostasis in response to nutritional stresses

Na Zhou,<sup>1,7,9</sup> Hailong Qi,<sup>2,9</sup> Junjun Liu,<sup>4,5,9</sup> Guangze Zhang,<sup>1</sup> Jianping Liu,<sup>8</sup> Ning Liu,<sup>1</sup> Minglu Zhu,<sup>1</sup> Xuyang Zhao,<sup>1</sup> Chang Song,<sup>1</sup> Zhe Zhou,<sup>1</sup> Jingjing Gong,<sup>1</sup> Ridong Li,<sup>1</sup> Xinyu Bai,<sup>1</sup> Yan Jin,<sup>1</sup> Yongfeng Song,<sup>4,5,6,\*</sup> and Yuxin Yin<sup>1,2,3,10,\*</sup>

<sup>1</sup>Institute of Systems Biomedicine, Department of Pathology, School of Basic Medical Sciences, Peking University Health Science Center, Beijing 100191, China

<sup>2</sup>Peking-Tsinghua Center for Life Sciences, Peking University Health Science Center, Beijing 100191, China

<sup>3</sup>Institute of Precision Medicine, Peking University Shenzhen Hospital, Shenzhen 518036, China

<sup>4</sup>Department of Endocrinology, Shandong Provincial Hospital Affiliated to Shandong First Medical University, Jinan, Shandong 250021, China

<sup>5</sup>Shandong Institute of Endocrine & Metabolic Diseases, Shandong First Medical University, Jinan, Shandong 250021, China

<sup>6</sup>Department of Endocrinology, Shandong Provincial Hospital, Cheeloo College of Medicine, Shandong University, Jinan, Shandong 250021, China

<sup>7</sup>Department of Clinical Laboratory, Shandong Provincial Hospital Affiliated to Shandong First Medical University, Jinan, Shandong 250021, China

<sup>8</sup>Department of Clinical Laboratory, The First Affiliated Hospital of Nanchang University, Nanchang, Jiangxi 330006, China

<sup>9</sup>These authors contributed equally

<sup>10</sup>Lead contact

\*Correspondence: [syf198506@163.com](mailto:syf198506@163.com) (Y.S.), [yinyuxin@bjmu.edu.cn](mailto:yinyuxin@bjmu.edu.cn) (Y.Y.)

<https://doi.org/10.1016/j.cmet.2022.05.005>

## SUMMARY

The ovarian-tumor-domain-containing deubiquitinases (OTUDs) block ubiquitin-dependent protein degradation and are involved in diverse signaling pathways. We discovered a rare *OTUD3* c.863G>A mutation in a family with an early age of onset of diabetes. This mutation reduces the stability and catalytic activity of OTUD3. We next constructed an experiment with *Otud3*<sup>-/-</sup> mice and found that they developed worse obesity, dyslipidemia, and insulin resistance than wild-type mice when challenged with a high-fat diet (HFD). We further found that glucose and fatty acids stimulate CREB-binding-protein-dependent OTUD3 acetylation, promoting its nuclear translocation, where OTUD3 regulates various genes involved in glucose and lipid metabolism and oxidative phosphorylation by stabilizing peroxisome-proliferator-activated receptor delta (PPAR $\delta$ ). Moreover, targeting PPAR $\delta$  using a specific agonist can partially rescue the phenotype of HFD-fed *Otud3*<sup>-/-</sup> mice. We propose that OTUD3 is an important regulator of energy metabolism and that the *OTUD3* c.863G>A is associated with obesity and a higher risk of diabetes.

## INTRODUCTION

Diabetes affects more than 400 million people worldwide and represents a substantial public health burden (Zheng et al., 2018). Obesity is one major risk factor because it results in insulin resistance that typically precedes diabetes (DeFronzo et al., 1992). Currently, genome-wide association studies (GWASs) have identified more than 80 diabetes-susceptibility loci (Mohlke and Boehnke, 2015). Moreover, increasing numbers of mutations and variants have been identified in monogenic forms of diabetes, e.g., maturity onset diabetes of the young (MODY)-like diabetes (Mohlke and Boehnke, 2015). The identification of genetic causes of diabetes mellitus provides useful information for the development of diagnostic screening tools and effective treatments and improves our understanding of the etiology and pathogenesis of this disease.

The ubiquitin (Ub) system is crucial for regulating protein turnover and is involved in the diverse signaling pathways associated with obesity and diabetes (Lee et al., 2000; Qi et al., 2006, 2008; Vecchione et al., 2003; Xu et al., 2008). Deubiquitylating enzymes (DUBs) remove Ub and regulate all Ub-dependent processes (Komander et al., 2009; Reyes-Turcu et al., 2009). More than 100 DUBs are found in human cells, which are involved in diseases such as neurodegenerative diseases, inflammation, infection, and cancer (Clague et al., 2012). The families of DUBs in the human proteome include Ub C-terminal hydrolases (UCHs), Ub-specific proteases (USPs), ovarian-tumor-related proteases (OTUs), machado-Joseph disease protein domain proteases (MJDs), Jab1/MPN-domain-associated metalloisopeptidase (JAMM) domain proteins, monocyte chemotactic-protein-induced proteins (MCPIPs), and the recently identified MINDYs (Rehman et al., 2016; Clague et al., 2013; Komander et al., 2009; Nijman et al., 2005). Ovarian-tumor-domain-containing

deubiquitinase 3 (OTUD3), a member of OTU deubiquitinase family, is ubiquitously expressed in the human body. OTUD3 signaling has been well described as a key regulator in tumorigenesis and innate immunity (Du et al., 2019; Yuan et al., 2015; Zhang et al., 2020). However, the involvement of OTUD3 in energy metabolism has not been investigated.

In this study, we report a novel, rare *OTUD3* c.863 G>A mutation identified by whole-exome sequencing in a family with an early age of onset of diabetes. The diabetes symptoms in affected family manifested in an autosomal dominant pattern. This mutation reduces the stability and catalytic activity of OTUD3 protein. More importantly, we found that glucose and fatty acids can stimulate CREB-binding protein (CBP)-dependent OTUD3 acetylation and promote its nuclear translocation, where OTUD3 regulates various genes involved in glucose and lipid metabolism and oxidative phosphorylation (OXPHOS) by stabilizing peroxisome-proliferator-activated receptor delta (PPAR $\delta$ ). Together, our data suggest that the CBP-OTUD3 signaling pathway may be a novel regulation mechanism for glucose and fatty acid metabolism.

## RESULTS

### Identification and characterization of an OTUD3 germline mutation in individuals with diabetes

Diabetes is a polygenic disorder with multiple genes located on different chromosomes contributing to its susceptibility (Zheng et al., 2018). To explore possible genetic causes of human diabetes, we identified a family comprised of 17 individuals from three generations with a high prevalence of early-onset inherited diabetes by autosomal dominant transmission as defined by the criteria of Roberts (Mohan et al., 2009) (Figure 1A). The age of onset of diabetes ranged from 9 to 50 years. Compared with healthy control subjects, the 4 affected individuals in this family showed increased fasting glucose levels and higher levels of glucose at 1 and 2 h in an oral glucose tolerance test (OGTT). But tests for glutamate decarboxylase and islet cell antibodies (indicators of type 1 diabetes) were negative (Table S1). None of the 4 affected individuals exhibited severe insulin deficiency (Table S1). This inherited trait prompted us to conduct a genetic screen. SNP array analysis identified eleven regions at chromosomes 1, 11, 14, and 17, which were shared by all 4 affected individuals, but not the healthy control (Table S2). The largest region of shared heterozygosity was at chromosome 1p34.1–36.13. Forty-one genes that had a maximum allele frequency (AF\_MAX) < 0.1 in normal control databases of different populations were sequenced (Table S2), while none of the 29 known monogenic diabetes genes (Ellard et al., 2013) were found. Therefore, there may be a new gene responsible for the 4 cases described above. A heterozygous missense substitution in exon 7 in the Ub-associated (UBA) domain of OTUD3 at chromosome 1p36.13 was detected in all affected individuals (NM\_015207: c.863 G>A: p.G288D), whereas none of the healthy siblings had this variant (Figure 1B).

We next screened for *OTUD3* mutations in 316 individuals with diabetes and 313 controls without diabetes. We found that the *OTUD3* c.863 G>A was a rare mutation (Figure 1C), which was detected only in individuals with diabetes (1.899% versus 0% in health control); all of the carriers were heterozygous. Correlation

test showed that the c.863 G>A heterozygous variant was significantly associated with human diabetes ( $p = 0.0305$ , OR = 0, 95% CI = 0–1.568) (Figure 1C). Furthermore, all the carriers have a history of being overweight (BMI > 25), and most of them have a BMI > 30. They showed impaired fasting glucose at the time of hospitalization. However, they are not associated with a significant dyslipidemia (Table S3). These results suggested a previously unappreciated link between *OTUD3* and human metabolic disease.

The *OTUD3* mutation c.863 G>A results in a non-conservative substitution of the glycine residue at 288 with a negatively charged aspartic acid (G288D) (Figure 1B). We first studied its impact on the stability of OTUD3. HEK293T cells were transfected with *OTUD3* wild-type (WT) or c.863 G>A mutant plasmid, followed by protein synthesis inhibitor cycloheximide (CHX) treatment. We found that the half-life of the G288D mutant was significantly lower compared with WT OTUD3 protein (Figure 1D, lanes 8–12 versus lanes 2–6). We next investigated whether the *OTUD3* c.863 G>A (G288D) mutation affects its deubiquitinase activity. PPAR $\delta$ , a new target of OTUD3 identified in this paper, and Ub were overexpressed in HEK293T cells to prepare over-ubiquitinated PPAR $\delta$  for cell-free deubiquitination assay. OTUD3 mutant (c.863 G>A, p.G288D) purified from *Escherichia coli* showed decreased DUB activity toward PPAR $\delta$  compared with WT OTUD3 (Figure 1E, lane 3 versus lane 2). PTEN (Yuan et al., 2015) and other targets of OTUD3 we identified also displayed similar results (Figure S1A–S1E, lane 3 versus lane 2). These data indicate that the *OTUD3* c.863 G>A results in a decrease in OTUD3 stability and its DUB activity.

### *Otud3*<sup>-/-</sup> mice present impaired energy metabolism and are predisposed to obesity and metabolic diseases

To understand the underlying mechanism of *OTUD3* c.863 G>A in the onset of diabetes, we attempted to create a mouse model carrying this mutation. However, as this segment of sequence is not conserved between human and mouse, we were unable to construct an identical mutation in mice. As *OTUD3* c.863 G>A leads to reduced protein stability and DUB activity, resulting in impaired function of OTUD3 in humans, we decided to construct *Otud3* knockout (KO) mice by application of CRISPR-Cas9. Two different founders of *Otud3* KO mice were obtained by introducing a base-deletion or -insertion-caused frameshift in exon 2 to avoid CRISPR off-target effects (Figure 2A). As shown in Figure S2A, OTUD3 is expressed in white adipose tissue (WAT), liver, and muscle tissues. Immunoblot analyses of liver, WAT, brown adipose tissue (BAT), and other tissues of mouse confirmed the completely deficiency of OTUD3 protein in *Otud3*<sup>-/-</sup> mice (Figure 2B, lanes 3, 4, 7, 8, 11, and 12 versus lanes 1, 2, 5, 6, 9, and 10; Figure S2B, lanes 4–6 versus lanes 1–3). No grossly visible dysplasia was observed in *Otud3*<sup>-/-</sup> mice, and their birth characteristics were in accordance with Mendel's inheritance law.

*Otud3*<sup>-/-</sup> and their control littermates (*Otud3*<sup>+/+</sup>) were fed either a normal diet (ND) (4% calories from fat) or a high-fat diet (HFD) (60% calories from fat) from the 8th week after their birth. After 10-week treatment, no significant body weight differences were observed in ND-fed *Otud3*<sup>-/-</sup> and *Otud3*<sup>+/+</sup> mice (Figure 2C). However, HFD-fed *Otud3*<sup>-/-</sup> mice gained more weight than *Otud3*<sup>+/+</sup> littermates (Figure 2C). The corporal proportions of retroperitoneal fat in HFD-fed *Otud3*<sup>-/-</sup> mice were higher than that of

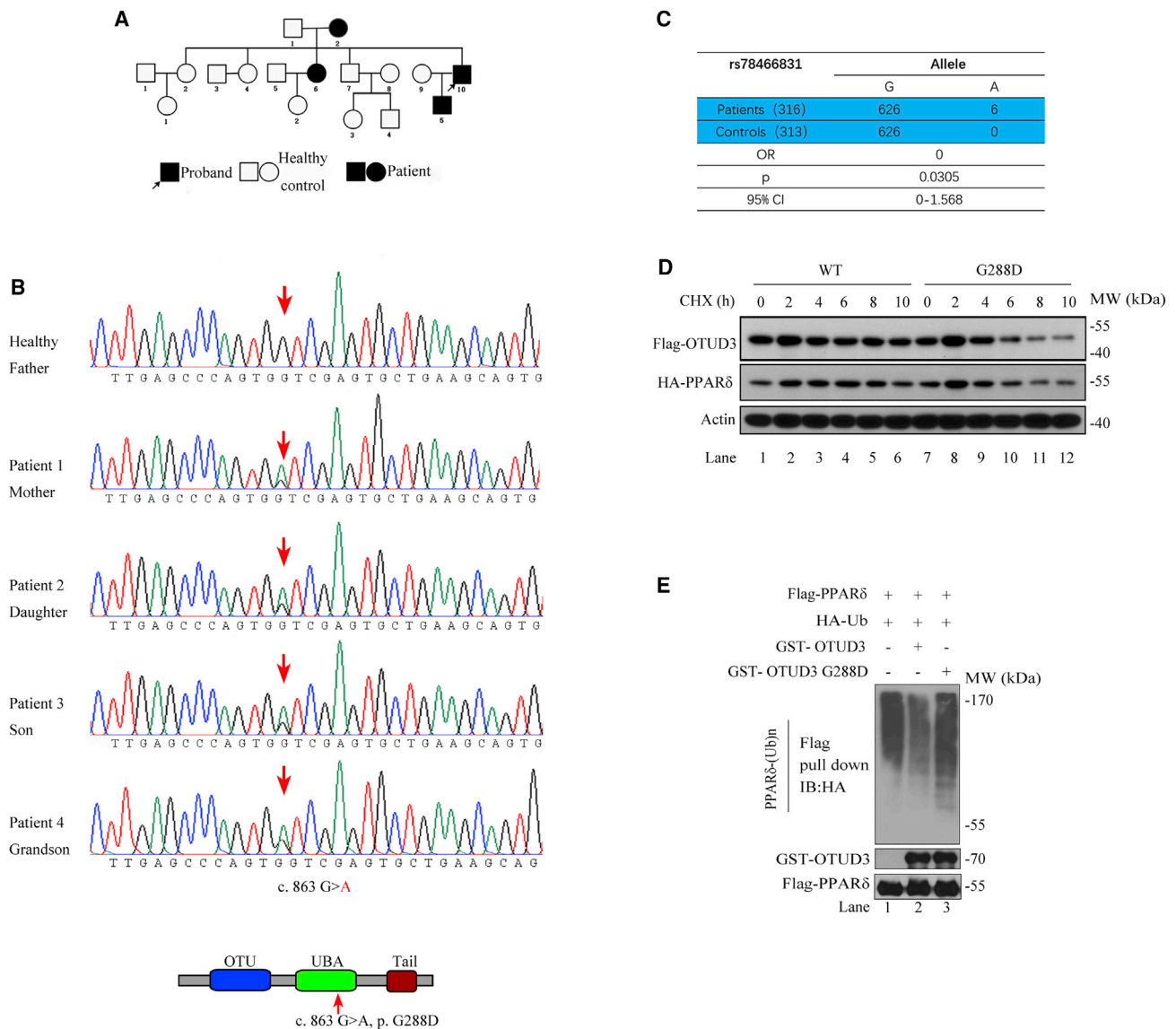


**Figure 1. Identification and characterization of c.863 G>A, p.G288D mutation of OTUD3**

(A) Family diagram of a MODY-like family. Proband is indicated with an arrow. The pedigree chart represents the MODY-like family.  $\circ$ , females;  $\square$ , males;  $\bullet$ , female with diabetes;  $\blacksquare$ , male with diabetes.

(B) *Otud3* DNA sequence chromatograms identifying the heterozygous single-base substitution mutation (c.863 G>A, p.G288D) located in the OTUD3 UBA domain (red arrow).

(C) A case-control study of *OTUD3* c.863 G>A mutation on 316 individual with diabetes and 313 individual without diabetes. Six *OTUD3* c.863 G>A, p.G288D carriers were discovered, and statistical analysis indicated that the mutation was associated with human diabetes.

(D) The G288D mutation is associated with reduced stability of PPAR $\delta$ . FLAG-tagged OTUD3 and HA-tagged PPAR $\delta$  were overexpressed in HEK293T cells and analyzed by immunoblotting using antibodies against HA and FLAG to indicate OTUD3 and PPAR $\delta$ , respectively. Cells were exposed to cycloheximide (CHX, 250  $\mu$ g/mL) for the indicated times.

(E) The G288D mutation decreases OTUD3 DUB activity toward PPAR $\delta$ . HEK293T cells were transfected with HA-Ub and FLAG-PPAR $\delta$ . Prior to collection, cells were exposed to a proteasome inhibitor MG132 (10  $\mu$ M) for 8 h. Cell lysates were immunoprecipitated with anti-FLAG beads, and the immunoprecipitant was incubated with purified GST-tagged wild-type OTUD3 and OTUD3 G288D mutant protein from *Escherichia coli* for 45 min at 37°C and immunoblotted with the anti-HA antibody to evaluate levels of ubiquitinated PPAR $\delta$ . The OTUD3 and PPAR $\delta$  levels in the input were evaluated by antibodies against GST and FLAG.

*Otud3*<sup>+/+</sup> littermates (Figures 2D and 2E). Accordingly, we found an increase in serum triglyceride (TG), free fatty acids (FFAs), and total and free cholesterol in the HFD-fed *Otud3*<sup>-/-</sup> mice compared with their *Otud3*<sup>+/+</sup> littermates (Figures 2F–2I). We also found an increase in fat accumulation in WAT, BAT, skeletal muscle, and liver

of *Otud3*<sup>-/-</sup> mice compared with *Otud3*<sup>+/+</sup> mice after 10 weeks of HFD feeding (Figures 2J and 2K). More importantly, we found the non-obese ND-fed *Otud3*<sup>-/-</sup> mice already showed increased accumulation of lipid droplet in muscle and liver by Oil Red O staining (Figure 2K).

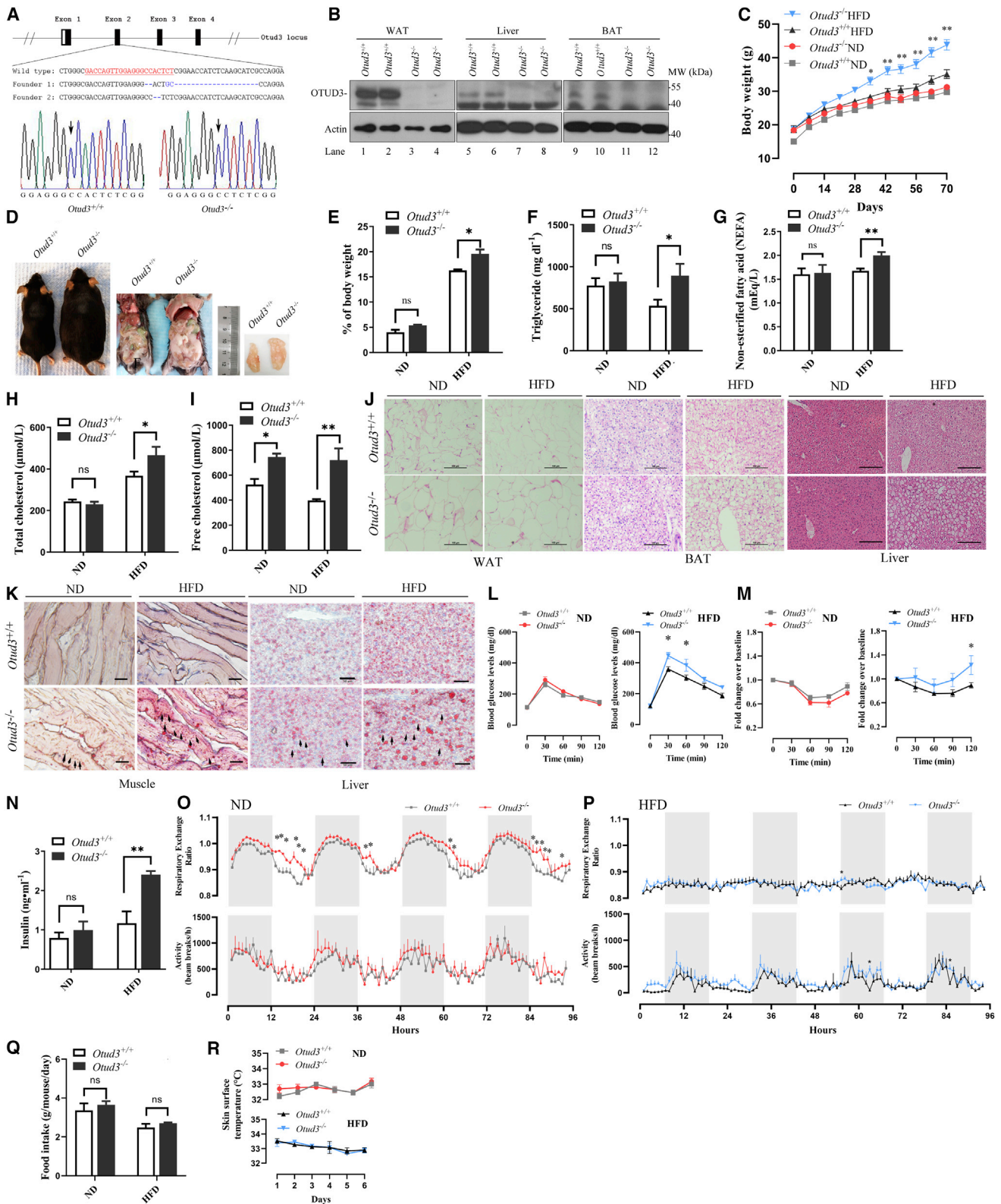


**Figure 2. *Otud3* knockout mice are prone to developing metabolic syndrome characterized by obesity, dyslipidemia, and insulin resistance** (A) *Otud3* knockout by the CRISPR-Cas9 technique. DNA sequence from exon 2 of wild-type and *Otud3* knockout mice was listed. CRISPR-Cas9-targeted sequence is highlighted in red. DNA sequences of *Otud3*<sup>-/-</sup> mice founder 1: the deleted letters indicate deleted sequence, and the blue letters indicate inserted sequence in homozygous mutant mice. DNA sequence of *Otud3*<sup>-/-</sup> mice founder 2: CRISPR-Cas9 introduced double base deletion causing frameshift mutation (legend continued on next page)

We next performed a glucose tolerance test (GTT) and insulin tolerance test (ITT) in *Otud3<sup>+/+</sup>* and *Otud3<sup>-/-</sup>* mice. We found a worse glucose intolerance and insulin resistance in the two founders of *Otud3<sup>-/-</sup>* mice after 10 weeks of HFD feeding compared with *Otud3<sup>+/+</sup>* littermates (Figures 2L, 2M, and S2C–S2F). The fasting serum insulin concentration was also higher in *Otud3<sup>-/-</sup>* mice fed an HFD compared with *Otud3<sup>+/+</sup>* littermates (Figure 2N).

Furthermore, impaired insulin signal transduction, as reflected by insulin-stimulated Akt phosphorylation, was found in WAT, muscle, and liver of *Otud3<sup>-/-</sup>* mice (Figures S2G–S2I, lane 6 versus lane 5 and lane 8 versus lane 7). Taken together, *Otud3<sup>-/-</sup>* mice are predisposed to obesity and develop worse glucose intolerance, insulin resistance, and dyslipidemia after metabolic challenge.

To explore why *Otud3<sup>-/-</sup>* mice are susceptible to HFD-induced obesity, we examined the food intake, body temperature, and energy expenditure using a metabolic cage. No significant alteration of  $VO_2$ ,  $VCO_2$ , respiratory exchange ratio (RER), or physical activity was found between ND-fed *Otud3<sup>-/-</sup>* and *Otud3<sup>+/+</sup>* mice during the dark periods (Figures 2O and S3A). The levels of these parameters began to decline in the light periods, where we found a significantly higher RER in *Otud3<sup>-/-</sup>* mice, while the other parameters were similar between the two groups (Figures 2O and S3A). We next investigated HFD-fed mice. Mice were placed in the metabolic cages and continued to receive an HFD. No remarkable difference was observed between the two groups. The RER was maintained at about 0.8 in both groups during the 1-week experiment (Figures 2P and S3B). No significant alterations in food intake and body surface temperature were found (Figures 2Q and 2R). These data imply a prefer-

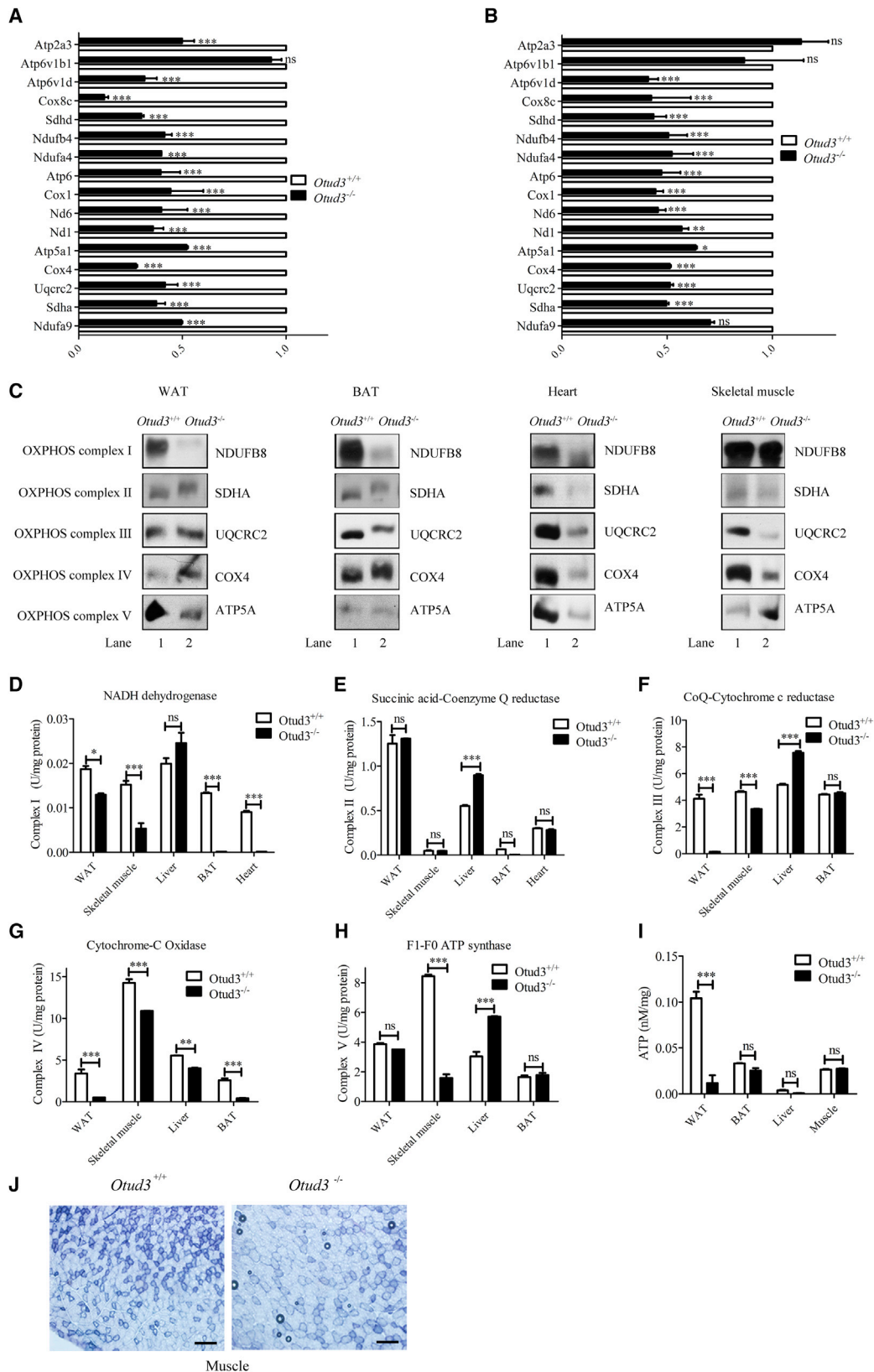
ence for carbohydrate fuel utilization of *Otud3<sup>-/-</sup>* mice and that the *Otud3<sup>-/-</sup>* mice could have a perturbation of FFA oxidation in key metabolic tissues.

As all of the c.863 G>A carriers were heterozygous, we also assayed the phenotype of heterozygous mice. There were no significant differences between the body weights of ND-fed *Otud3<sup>+/-</sup>* mice and *Otud3<sup>-/-</sup>* or *Otud3<sup>+/+</sup>* mice (Figure S3C). When challenged with an HFD, the *Otud3<sup>+/-</sup>* mice showed a similar tendency to *Otud3<sup>-/-</sup>* mice to gain significantly more weight than *Otud3<sup>+/+</sup>* mice (Figure S3D). Furthermore, the ND-fed *Otud3<sup>+/-</sup>* mice showed a mixed phenotype with regard to RER between the *Otud3<sup>-/-</sup>* and *Otud3<sup>+/+</sup>* (Figure S3A). The HFD-fed *Otud3<sup>+/-</sup>* mice showed a comparable RER versus the HFD-fed *Otud3<sup>-/-</sup>* and *Otud3<sup>+/+</sup>* (Figure S3B). No significant alteration in  $VO_2$ ,  $VCO_2$ , physical activity, food intake, and body surface temperature values was found in *Otud3<sup>+/-</sup>* mice fed either ND or HFD compared with those in *Otud3<sup>-/-</sup>* and *Otud3<sup>+/+</sup>* mice during the light periods (Figures S3A, S3B, and S3E–S3G).

Additionally, the ND-fed *Otud3<sup>+/-</sup>* mice showed no significant difference in glucose tolerance and insulin resistance compared with either *Otud3<sup>-/-</sup>* or *Otud3<sup>+/+</sup>* mice (Figures S3H and S3I). After challenge with an HFD, the *Otud3<sup>+/-</sup>* mice showed an increased glycemia profile by GTT compared to *Otud3<sup>+/+</sup>*, but the differences were non-significant compared with either *Otud3<sup>-/-</sup>* or *Otud3<sup>+/+</sup>* mice (Figures S3J and S3K). The result of ITTs showed that *Otud3<sup>+/-</sup>* mice fed an HFD developed worse insulin resistance compared with *Otud3<sup>+/+</sup>* mice, and their glycemia profile was comparable to *Otud3<sup>-/-</sup>* mice. Taken together, *Otud3*-deficient mice are predisposed to obesity and develop worse glucose intolerance, insulin resistance, and dyslipidemia after metabolic challenge.

- to disrupt OTUD3 protein of *Otud3<sup>-/-</sup>* mice. Genotyping of *Otud3* wild-type (*Otud3<sup>+/+</sup>*) and homozygous mutated (*Otud3<sup>-/-</sup>*) of mice founder 2: the *Otud3<sup>+/+</sup>* chromatogram is shown on the left, and the chromatogram from a homozygous mutant is shown on the right.
- (B) Immunoblot confirmation of the elimination of OTUD3 in WAT, BAT, and liver from *Otud3<sup>-/-</sup>* mice. Protein extracts from WAT, BAT, and liver of representative two pairs of *Otud3<sup>+/+</sup>* and *Otud3<sup>-/-</sup>* mice were immunoblotted with the anti-OTUD3 antibody (Sigma, HPA028543) and anti- $\beta$ -actin (MBL, #PM053). Each lane was loaded with an equivalent weight of tissue.
- (C) Body weights of ND- and HFD-fed *Otud3<sup>+/+</sup>* and *Otud3<sup>-/-</sup>* mice of founder 2. Body weights of *Otud3<sup>+/+</sup>* and *Otud3<sup>-/-</sup>* mice were measured twice a week for 10 weeks (n = 7 for each group).
- (D) Effects of *Otud3* knockout on body size and adipose tissue size. The photographs show body size (left), view of ventral adipose tissues (middle), and size of epididymal adipose tissues (right) in HFD-fed *Otud3<sup>+/+</sup>* and *Otud3<sup>-/-</sup>* mice.
- (E) Weights of epididymal adipose tissues normalized by body weight in ND- and HFD-fed *Otud3<sup>+/+</sup>* and *Otud3<sup>-/-</sup>* mice for 10 weeks (n = 4 mice per group).
- (F) Serum triglyceride levels (mg/dL) in ND- and HFD-fed *Otud3<sup>+/+</sup>* mice and *Otud3<sup>-/-</sup>* (n = 10 mice per group).
- (G) Serum non-esterified fatty acid (NEFA) levels (mEq/L) in ND- and HFD-fed *Otud3<sup>+/+</sup>* and *Otud3<sup>-/-</sup>* (n = 7 mice per group).
- (H and I) Serum free and total cholesterol levels ( $\mu$ mol/L) in ND- and HFD-fed *Otud3<sup>+/+</sup>* and *Otud3<sup>-/-</sup>* mice (n = 6 mice per group).
- (J) Representative H&E staining of BAT, WAT, and livers of ND- and HFD-fed *Otud3<sup>+/+</sup>* and *Otud3<sup>-/-</sup>* mice. White adipocyte hypertrophy: more and larger vacuoles appear in BAT and livers of *Otud3<sup>-/-</sup>* mice after being fed an HFD for 10 weeks (n = 3 mice per group). Scale bars, 100  $\mu$ m.
- (K) Representative Oil Red O staining of liver and red muscle of ND- and HFD-fed *Otud3<sup>+/+</sup>* and *Otud3<sup>-/-</sup>* mice. Black arrows indicate oil droplets. Increased oil droplets in red muscle and liver of *Otud3<sup>-/-</sup>* mice after 10 weeks feeding on an HFD (n = 3 mice per group). Scale bars, 50  $\mu$ m.
- (L and M) GTTs and ITTs of ND- and HFD-fed *Otud3<sup>+/+</sup>* and *Otud3<sup>-/-</sup>* mice of founder 2. Mice were challenged by 2 g/kg glucose or 0.8 U/kg insulin (regular insulin, Wanbang) via intraperitoneal (i.p.) injection (n = 4 for each group).
- (N) Serum insulin levels of *Otud3<sup>-/-</sup>* and *Otud3<sup>+/+</sup>* mice. Serum insulin levels at 10 a.m. were tested by an ELISA (n = 10 mice per group). ns, p = 0.3716; \*\*p = 0.0031 (paired Student's t test).
- (O) Respiratory exchange ratio (RER) and activities of ND-fed *Otud3<sup>+/+</sup>* and *Otud3<sup>-/-</sup>* mice of founder 2. Mice were put individually into a metabolic cage. The  $VO_2$ ,  $VCO_2$ , and activities were measured by built-in detector. RER was calculated by dividing  $VCO_2/VO_2$  (n = 4 for each group).
- (P) RER and activities of HFD-fed *Otud3<sup>+/+</sup>* and *Otud3<sup>-/-</sup>* mice (n = 4 for each group; missing data in the HFD-fed *Otud3<sup>+/+</sup>* group due to equipment failure).
- (Q) Daily food intake of ND- and HFD-fed *Otud3<sup>+/+</sup>* and *Otud3<sup>-/-</sup>* mice. Mice were put individually into a metabolic cage. The food intake was measured by built-in detector (n = 4 for each group).
- (R) Skin surface temperatures of ND- and HFD-fed *Otud3<sup>+/+</sup>* and *Otud3<sup>-/-</sup>* mice. The temperatures were measured at 16 h every day by infrared imaging (n = 4 for each group).

Data are presented as mean  $\pm$  SEM. \*p < 0.05, \*\*p < 0.01, \*\*\*p < 0.001 by two-way ANOVA.



(legend on next page)

### OTUD3 loss of function results in a decrease in oxidative phosphorylation capacity

To confirm whether the *Otud3*<sup>-/-</sup> mice are associated with decreased oxidative metabolism, we first measured the expression levels of genes involved in the respiratory chain using the primer sets listed in Table 1. qRT-PCR results showed that WAT and skeletal muscle tissues of *Otud3*<sup>-/-</sup> mice were less oxidative compared with *Otud3*<sup>+/+</sup> control (Figures 3A and 3B). We further analyzed the mitochondrial respiratory chain complexes using BN-PAGE and immunoblotting. Most of the expression levels of OXPHOS subunits were decreased in isolated mitochondria from most of metabolic tissues of *Otud3*<sup>-/-</sup> mice (Figure 3C, lane 2 versus lane 1). We also compared the mitochondrial respiration chain complex activities in WAT, BAT, liver, and skeletal muscle between 5-month-old HFD-fed *Otud3*<sup>-/-</sup> and *Otud3*<sup>+/+</sup> mice. We found that the activities were significantly decreased in the *Otud3*<sup>-/-</sup> mouse tissues compared with *Otud3*<sup>+/+</sup> mice, except complex II (Figures 3D–3H). Accordingly, cellular ATP levels were significantly lower in WAT of *Otud3*<sup>-/-</sup> mice compared with *Otud3*<sup>+/+</sup> (Figure 3I). NADH-tetrazolium reductase (NADH-TR) staining also showed fewer oxidative muscle fibers in *Otud3*<sup>-/-</sup> mice than *Otud3*<sup>+/+</sup> mice (Figure 3J).

To provide more comprehensive evidence of the potential role of OTUD3 in energy metabolism, we assessed the impact of OTUD3 knockdown on glucose uptake, lactate generation, oxygen consumption rate (OCR), and extracellular acidification rate (ECAR) assays in 3T3-L1 cells after differentiation. Two different OTUD3 knockdown stable cell lines were established by lentiviral transfection prior to differentiation (Figure S4A, lanes 3 and 4 versus lane 2). We found reduced glucose uptake and increased lactate production (Figures S4B and S4C) in differentiated *Otud3* knockdown 3T3-L1 cells compared with scramble shRNA (Con shRNA). Targeting metabolic analysis also showed that the levels of citrate, fumaric acid, succinate, and acetyl-CoA were decreased in WAT tissue of *Otud3*<sup>-/-</sup> mice compared with *Otud3*<sup>+/+</sup> (Figure S4D), which were associated with a lower OCR and higher ECAR (Figures S4E–S4H).

We further investigated whether carriers of the *OTUD3* c.863G>A mutation were also associated with mitochondrial dysfunction. Peripheral blood mononuclear cells (PBMCs) were collected for evaluating OXPHOS gene expression levels. We found that the expression levels of most OXPHOS genes were significantly decreased in PBMCs of carriers compared with healthy controls (Figure S4I). Accordingly, we found reduced ATP production in 3T3-L1 cells infected with G288D mutant compared with those infected with WT OTUD3 (Figure S4J). We then analyzed the impact of G288D mutant on 3T3-L1 cells'

mitochondrial complexes I–V enzyme activity, and a decrease of the activities of complexes I, III, and V was detected (Figure S4K). Targeted mass spectrometry assay revealed that these cells catabolize less oleic acid than those transfected with WT OTUD3 (Figure S4L). Collectively, these data indicate that OTUD3 is important in maintaining the expression of key OXPHOS genes. OTUD3 loss of function or *OTUD3* c.863G>A mutation results in a decreased OXPHOS capacity.

### OTUD3 is involved in the energy metabolism regulation process

To better understand the general effects of *Otud3* loss of function in adipocytes, we performed an RNA sequencing (RNA-seq) analysis on the WAT samples of HFD-fed mice. We found 282 downregulated genes and 16 upregulated genes in WAT from *Otud3*<sup>-/-</sup> mice compared with *Otud3*<sup>+/+</sup> mice (Figure 4A). We generated a heatmap of these pathway-related genes (Figure 4B), which were then further validated by qRT-PCR (Figure 4C). Gene set enrichment analysis of *Otud3* loss-of-function-related genes scored highly under diabetes, PPAR signaling pathway, glycolipid metabolism, and fatty acid degradation (Figure S5A; Table S4). These pathways are potentially involved in the obese phenotype of *Otud3*<sup>-/-</sup> mice.

Our RNA-seq data revealed a number of genes affected by the loss of function of OTUD3. However, as a deubiquitinase, OTUD3 does not directly regulate the genes' expression; it functions through regulating the turnover of its substrates. To further identify potential transcriptional regulators (i.e., OTUD3 substrates) responsible for these changes, we performed chromatin immunoprecipitation sequencing (ChIP-seq) analysis using WAT of mice overexpressing FLAG-tagged OTUD3. KEGG pathway enrichment analysis showed that metabolic pathway, PI3K, insulin signaling pathway, and OXPHOS are enriched pathways (Figure S5B; Table S5). We next carried out the integration of RNA-seq and ChIP-seq data and found 52 overlapping genes ( $p < 0.05$ ) between RNA-seq of differentially expressed and ChIP-seq of OTUD3-bound genes (Figure 4D). A panel of 26 nuclear OTUD3 target genes from the ChIP-seq data, which also displayed decreased mRNA expression levels as determined by RNA-seq, were followed by ChEA3 analysis (Keenan et al., 2019) (Figure 4E). The resulting list of proteins from ChEA3 analysis contained candidate cofactors for OTUD3 (Table S6), such as FOXN1 (Kuschnerus et al., 2019), FOXA2 (Bastidas-Ponce et al., 2017), hepatocyte nuclear factor 1 $\beta$  (HNF1B) (Dubois-Laforgue et al., 2017), HOXB8 (Karastergiou et al., 2013), SIX3 (Arda et al., 2016), and BHLHE22 (Melkman-Zehavi et al., 2011). We next performed co-immunoprecipitation assays to

#### Figure 3. Impaired oxidative phosphorylation in metabolic-associated tissues in *Otud3*<sup>-/-</sup> mice

(A and B) mRNA levels of OXPHOS subunits were analyzed by qRT-PCR in WAT and skeletal muscle tissues of *Otud3*<sup>+/+</sup> and *Otud3*<sup>-/-</sup> mice (n = 4 mice per group). Data were normalized with *Actin* mRNA levels.  
(C) Representative immunoblots of the OXPHOS complex subunits NDUFB8, SDHA, UQCRC2, COX4, and ATP5A in WAT, BAT, skeletal muscle, and heart tissues of *Otud3*<sup>+/+</sup> and *Otud3*<sup>-/-</sup> mice using BN-PAGE. Each lane was loaded with an equivalent weight of lysates.  
(D–H) Respiratory chain activity in isolated mitochondria from WAT, BAT, skeletal muscle, liver, and heart tissues of *Otud3*<sup>+/+</sup> and *Otud3*<sup>-/-</sup> mice. Mitochondrial complex activities of these tissues were measured (n = 4 mice for each group).  
(I) Whole ATP content in WAT, BAT, liver, and skeletal muscle tissues of *Otud3*<sup>+/+</sup> and *Otud3*<sup>-/-</sup> mice by ATP assay kit (n = 4 mice for each group).  
(J) NADH-tetrazolium reductase histochemical staining of tibialis muscle of 20-week-old *Otud3*<sup>+/+</sup> and *Otud3*<sup>-/-</sup> mice. Oxidative and intermediate fibers were darkly and moderately stained, while glycolytic fibers were unstained. Scale bars, 100  $\mu$ m.  
Data are presented as mean  $\pm$  SEM. \* $p < 0.05$ , \*\* $p < 0.01$ , \*\*\* $p < 0.001$  (two-way ANOVA).



confirm the interaction between OTUD3 and these metabolic related transcriptional regulators. In HEK293T cells co-transfected with exogenous OTUD3 and FLAG-tagged transcriptional regulators, we found increased levels of OTUD3 in the immunoprecipitants of these transcriptional regulator groups compared to the vector group (Figure S5C, lanes 2–7 versus lane 1). Also, increased levels of endogenous OTUD3 were found in most of the immunoprecipitants of transcription regulators compared to IgG (Figures S5D–S5I, lane 1 versus lane 2). Ubiquitination assays showed that OTUD3 overexpression decreased the ubiquitination levels of these transcription regulators (Figures 4F–4K, lane 3 versus lane 2; Figure 4L, lanes 2, 4, 6, 8, 10, and 12 versus lanes 1, 3, 5, 7, 9, and 11). These data indicate that OTUD3 is involved in the regulation of metabolic homeostasis through interacting with diverse cofactors.

### OTUD3 interacts with and stabilizes PPAR $\delta$ through deubiquitination

OTUD3 has a broad substrate spectrum. Considering the obese phenotype, the decreased PPAR signaling pathway gene expression, and the defected OXPHOS in WAT and muscle of the *Otud3*<sup>-/-</sup> mice, we further investigated PPAR $\delta$ , a key mediator of energy metabolism in adipose tissues. Moreover, the phenotype of our *Otud3*<sup>-/-</sup> mice is very similar to that of PPAR $\delta$ -deficient mice (Wang et al., 2003). Co-immunoprecipitation assays were carried out using extracts of 3T3-L1 cells (Figure 5A) and HEK293T cells (Figure 5B). PPAR $\delta$  was co-immunoprecipitated with both endogenous OTUD3 (Figure 5A, lane 1 versus lane 2) and exogenous OTUD3 (Figure 5B, lanes 2–4 versus lane 1). To map the PPAR $\delta$ -binding domain of OTUD3, FLAG-tagged fragments corresponding to the three domains of OTUD3 were co-expressed in HEK293T cells with HA-tagged PPAR $\delta$ . Subsequent co-immunoprecipitation assays showed that only the NH<sub>2</sub>-terminal OTU domain of OTUD3 was required for physical interaction with PPAR $\delta$  (Figure S6A, lanes 3–6 versus lane 2). Conversely, both the transactivation and ligand-binding domains of PPAR $\delta$  were required for binding to OTUD3 NH<sub>2</sub> terminus. (Figure S6B, lane 4 versus lanes 2 and 6). Furthermore, we found glucose promoted the interaction between OTUD3 and PPAR $\delta$  (Figure 5B, exogenous OTUD3, lanes 3 and 4 versus lane 2; Figure 5C, endogenous OTUD3, lanes 3–5 versus lane 2).

Next, we investigated the impact of OTUD3 deficiency on PPAR $\delta$  protein levels. We found that PPAR $\delta$  was markedly decreased in *Otud3* knockdown 3T3-L1 cells (Figure 5D, lanes 2 and 3 versus lane 1). Also, PPAR $\delta$  was decreased in the skeletal tissue and WAT of *Otud3*<sup>-/-</sup> mice (Figure 5E, lanes 3 and 4 versus lanes 1 and 2; lanes 7 and 8 versus lanes 5 and 6). Moreover, ectopic expression of OTUD3 resulted in a dose-depend-

ent increase of PPAR $\delta$  levels (Figure S6C, lanes 2–4 versus lanes 1 and 5). Accordingly, the half-life of PPAR $\delta$  was significantly decreased in *Otud3* knockdown 3T3-L1 cells (Figure 5F, lanes 6–8 versus lanes 2–4). PPAR $\delta$  protein levels increased as the glucose concentration increased, which was abolished in OTUD3 KO 3T3-L1 cells (Figure 5G, lanes 4–6 versus lanes 1–3). Finally, PPAR $\delta$ -controlled genes required for oxidation in adipose tissue were also expressed at lower levels in *Otud3*<sup>-/-</sup> mice (Figure 5H).

Ubiquitination assays showed purified OTUD3 protein directly removes the Ub chain from PPAR $\delta$  (Figure 1E, lane 3 versus lane 2). Consistent with this finding, knockdown of *Otud3* in HEK293T cells showed increased ubiquitination levels of PPAR $\delta$  (Figure S6D, lanes 2 and 3 versus lane 1), and exogenous expression of WT OTUD3, but not the G288D mutant, in OTUD3 KO cells reduced the ubiquitination levels of PPAR $\delta$  (Figure 5I, lane 3 versus lane 2). More specifically, OTUD3 removed Lys 48-linked polyubiquitination, which acts mainly to target cargo for proteasome degradation (Figure 5J, lane 4 versus lane 3).

Additionally, to confirm the role of PPAR $\delta$  in the obese phenotype of *Otud3*<sup>-/-</sup> mice, we performed a rescue experiment using the PPAR $\delta$  agonist GW501516 to boost the remnant PPAR $\delta$  activity. We evaluated the rescue effect of agonist by comparing the HFD-fed *Otud3*<sup>-/-</sup> mice with and without GW501516 supplement. The *Otud3*<sup>-/-</sup> mice fed an HFD were treated with either vehicle or GW501516 (5 mg/kg/day) for 7 weeks. Vehicle-treated HFD-fed *Otud3*<sup>-/-</sup> mice developed glucose intolerance and insulin resistance. In contrast, GW501516-treated HFD-fed *Otud3*<sup>-/-</sup> mice showed a significant reduction in weight gain compared with vehicle (Figure 5K). GTTs and ITTs also showed that GW501516 improved glucose tolerance and insulin resistance compared with vehicle (Figures 5L and 5M). These findings reinforce our hypothesis that PPAR $\delta$  is a key target of OTUD3, and that its dysfunction plays an indispensable role in the pathogenesis of metabolic syndrome in *Otud3*<sup>-/-</sup> mice.

### Glucose and fatty acids stimulate OTUD3 nuclear translocation through CREB-binding-protein-mediated acetylation

The nuclear receptor PPAR $\delta$  and the other OTUD3 target transcription factors are localized mainly in nuclei (Manickam and Wahli, 2017); in contrast, OTUD3 has been previously reported to be localized in cytoplasm (Yuan et al., 2015). We found a similar result that the endogenous OTUD3 was localized mainly in cytoplasm at basal condition. However, nuclear endogenous OTUD3 levels increased with FFA (Figure 6A, lanes 8–12 versus lane 7) or glucose (Figure S7A, lanes 9–11 versus lanes 7 and 8) stimulation in a dose-dependent manner in 3T3-L1 cells. The

(B) Heatmap of RNA-seq showed changes in the expression of the indicated fatty acids and glucose-metabolism-related genes. [ $\log_2$ fold change] > 1.5 and  $p < 0.05$ .

(C) qRT-PCR analysis showed that PPAR- and fatty acid oxidation metabolic pathway-related genes decreased in WAT of *Otud3*<sup>-/-</sup> mice compared with *Otud3*<sup>+/+</sup> mice in accordance with RNA-seq results ( $n = 3$  mice for each group). Bars represent mean  $\pm$  SEM. \* $p < 0.05$ , \*\* $p < 0.01$ , \*\*\* $p < 0.001$  (two-way ANOVA).

(D) Venn diagram of 52 overlapped genes ( $p < 0.05$ ) between RNA-seq of differentially expressed genes and ChIP-seq of OTUD3-bound genes.

(E) Overlap of downregulated RNA-seq genes of *Otud3*<sup>-/-</sup> group and ChIP-seq targets ( $p < 0.05$ ).

(F–K) Intracellular transcriptional regulator ubiquitination assay. HEK293T cells were co-transfected with His-HA-ubiquitin (Ub), FLAG-tagged transcriptional regulators, and Myc-tagged OTUD3 plasmids. Lysates were immunoprecipitated with anti-FLAG beads and immunoblotted with anti-HA and FLAG antibodies. Cells were treated with MG132 (10  $\mu$ M) for 8 h before harvest.

(L) Transcriptional regulator ubiquitination assay. HEK293T cells transfected with indicated plasmids were treated with MG132 (10  $\mu$ M) for 8 h before collection. The whole-cell lysates were immunoprecipitated with anti-FLAG beads and incubated with purified GST-OTUD3 at 37°C for 1 h.

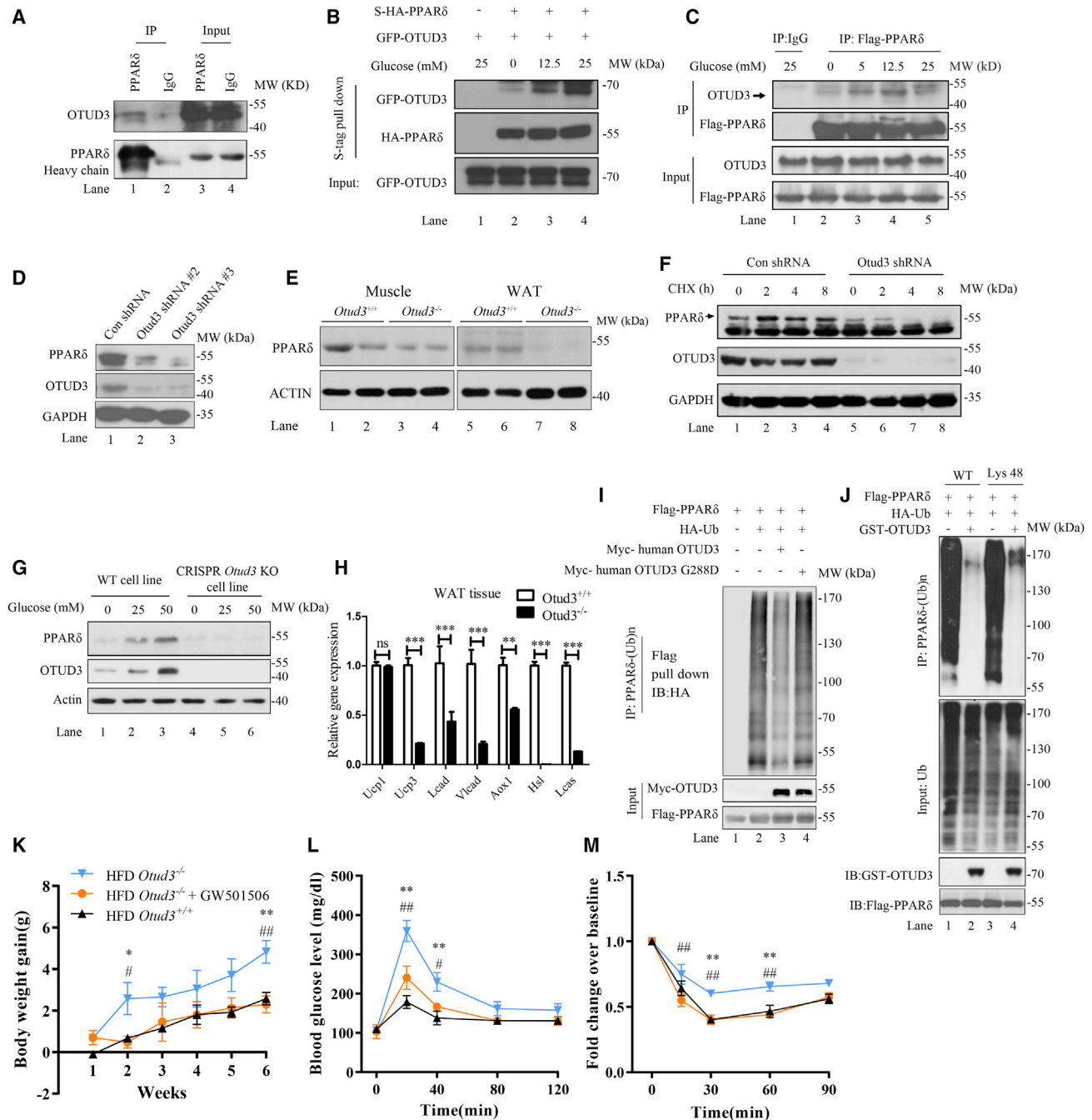


**Figure 5. OTUD3 directly interacts with and deubiquitinates PPAR $\delta$**

(A) Intracellular interaction between PPAR $\delta$  and OTUD3. Endogenous PPAR $\delta$  was immunoprecipitated from 3T3-L1 cell lysates and immunoblotted with antibodies against OTUD3 and PPAR $\delta$ , respectively.

(B) Glucose enhances the binding between exogenous OTUD3 and PPAR $\delta$ . HEK293T cells were co-transfected with GFP-OTUD3, PSAN-PPAR $\delta$  (contains both HA-tag and S-tag), or PSAN-vector and treated with increasing glucose concentrations (0, 12.5, and 25 mM) for 8 h. PPAR $\delta$  was immunoprecipitated from cell lysates using S-protein beads, and the immunoprecipitants were immunoblotted with antibodies against the HA or GFP to reveal PPAR $\delta$  and OTUD3.

(C) Glucose enhances the binding between endogenous OTUD3 and PPAR $\delta$ . 3T3-L1 cells were infected by adenovirus-FLAG-PPAR $\delta$  and treated with increasing glucose concentrations (0, 5, 12.5, and 25 mM) for 8 h. PPAR $\delta$  was immunoprecipitated by CST rabbit anti-FLAG antibody and revealed by Sigma mouse anti-FLAG M2 antibody. OTUD3 was revealed by antibody against OTUD3.

(D) Immunoblotting of PPAR $\delta$  in lentivirus-mediated *Otud3* knockdown 3T3-L1 stable cell lines using the antibody against PPAR $\delta$  (Santa Cruz, sc-7197).

(E) Immunoblot analysis of skeletal muscle and WAT of *Otud3*<sup>+/+</sup> and *Otud3*<sup>-/-</sup> mice using the antibody against PPAR $\delta$  (Abcam, ab23673) and actin (MBL, #PM053). Representative result from two pairs of littermates was shown.

(legend continued on next page)

nuclear translocation of OTUD3 in response to glucose or FFA stimulation was further confirmed by immunofluorescence (Figure 6B) and live-cell imaging (Figure S7B).

To understand the mechanism for OTUD3 nuclear translocation, we use high-resolution mass spectrometry to analyze the post-translational modifications of OTUD3. We found that OTUD3 was highly acetylated at a number of acetylation sites under 25 mM glucose (Table S7). The acetylation sites were mapped in Table S7. Next, OTUD3 was immunoprecipitated from cell lysates of 3T3-L1 cells cultured under increasing glucose or FFA levels. We found that both glucose and FFA significantly increased OTUD3 acetylation levels in a dose-dependent manner (Figure 6C, lanes 2–4 versus lane 1; Figure S7C, lanes 2–4 versus lane 1). ACLY inhibitor SB 204990 remarkably attenuated both glucose- and FFA-stimulated OTUD3 acetylation (Figures 6C and S7C, lanes 6–8 versus lanes 2–4). Enhanced OTUD3 acetylation was observed upon acetyl-CoA treatment (Figure S7D, lanes 2–4 versus lane 1).

CBP is an important acetyltransferase that regulates energy metabolism (Dancy and Cole, 2015). To investigate its potential effects on OTUD3 acetylation, CBP was overexpressed in HEK293T cells. We found that the acetylation levels of OTUD3 significantly increased by the ectopic expression of CBP in a dose-dependent manner (Figure 6D, lanes 2–4 versus lane 1). However, without glucose (0 mM), CBP cannot acetylate OTUD3 (Figure 6D, lane 5 versus lane 4). siRNA-mediated CBP knockdown reduced the acetylation levels of OTUD3 (Figure S7E, lanes 2 and 3 versus lanes 5 and 6). As GCN5 is one of the most acetyl-CoA-sensitive HATs, we also tested whether OTUD3 acetylation might be GCN5 dependent. However, GCN5 failed to increase OTUD3 acetylation levels (Figure S7F, lanes 3–6 versus lanes 1 and 2).

We next investigated the role of CBP in OTUD3 translocation. We overexpressed CBP in HEK293T cells maintained in normal DMEM medium (25 mM glucose) and found that ectopic CBP expression promoted nuclear translocation of OTUD3 (Figure 6E, lane 4 versus lane 3). We also tested the effects of the histone deacetylase inhibitor TSA and the sirtuin inhibitors TSA and NAM. We found that TSA, but not NAM, significantly increased the acetylation level of OTUD3 in 3T3-L1 cells (Figure 6F, lanes 2 and 4 versus lane 1). TSA also increased nuclear accumulation

of OTUD3 (Figure 6G, lanes 7 and 8 versus lane 5). These results demonstrate that high levels of glucose or fatty acids trigger the activation of CBP, leading to increased levels of acetylation of OTUD3, which facilitates its nuclear translocation.

Furthermore, both glucose and fatty acids increased CBP acetylation levels in a dose-dependent manner, which was associated with an increase in CBP acetyltransferase activity (Figure S7G, lanes 3 and 4 versus lane 2; Figure S7H, lane 3 versus lane 2). Also, increased interaction between CBP and OTUD3 was correlated with increases in glucose and fatty acid concentrations (Figure S7I, lanes 3–5 versus lane 2). These data indicate that CBP linked the glucose and fatty acid overload with OTUD3 acetylation status (Figure 6H).

To identify the primary acetylation site(s) of OTUD3, the lysine residues in the UBA domain were replaced one by one by arginine. However, none of the single-substituted lysine mutants exhibited lower levels of overall acetylation than those observed with WT OTUD3 (data not shown). We then generated OTUD3 mutants with multiple substitution. We found that OTUD3 acetylation levels were decreased significantly when nine lysine residues were replaced with arginine (9KR) (Figure S7J, lane 4 versus lane 3 and lane 2 versus lane 1). To further confirm the indispensable role of acetylation for OTUD3 nuclear translocation, HEK293T cells were transfected with WT OTUD3 and 9KR mutant. The subcellular localization of these proteins was evaluated by immunoblotting of nuclear and cytosolic fractions with and without glucose stimulation. We found the nuclear levels of the 9KR mutant were significantly lower than WT OTUD3 in the presence and absence of glucose (Figure S7K, lane 8 versus lane 4 and lane 7 versus lane 3). These results confirm that the nuclear translocation of OTUD3 is dependent on its acetylation levels.

Next, we investigated whether 9KR mutation affected its deubiquitination activity to PPAR $\delta$ . The HEK293T *Otud3* KO cells were transfected with WT *Otud3* and 9KR mutant. They were also co-transfected with FLAG-tagged PPAR $\delta$  and HA-tagged Ub. The PPAR $\delta$  was enriched by immunoprecipitation using anti-FLAG beads, and the ubiquitylation levels of PPAR $\delta$  were revealed using anti-HA antibody. We found that cells transfected with the 9KR mutant showed an increase in ubiquitylation levels of PPAR $\delta$  compared with WT OTUD3 (Figure S7L, lane 4 versus

(F) Half-life analysis of PPAR $\delta$  in *Otud3* knockdown 3T3-L1 cells. *Otud3 shRNA* and *Con shRNA* lentivirus-stable-transfected 3T3-L1 cell lines were exposed to cycloheximide (CHX, 250  $\mu$ g/mL) at the times indicated. Levels of PPAR $\delta$  and OTUD3 protein in *Otud3 shRNA* and *Con shRNA* 3T3-L1 cells were analyzed by immunoblotting using antibodies against PPAR $\delta$  (Santa Cruz, sc-7197) and OTUD3, respectively.

(G) Protein levels of PPAR $\delta$  and OTUD3 after exposure to increasing glucose concentration. WT and *Otud3* CRISPR KO 3T3-L1 cells were incubated in different concentrations of glucose (0, 25, and 50 mM) for 8 h. Levels of PPAR $\delta$  (Abcam, ab23673) and OTUD3 protein were analyzed by immunoblotting.

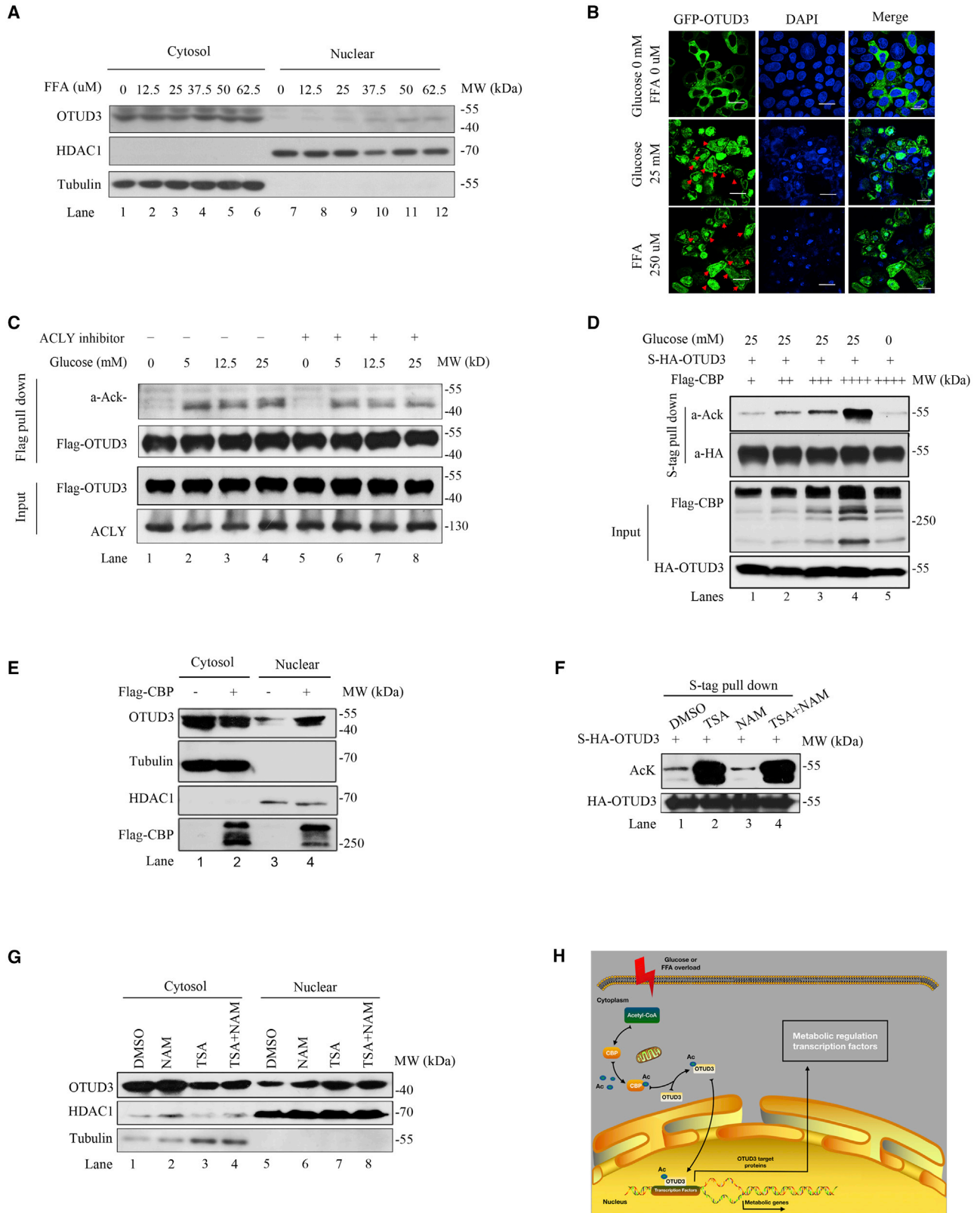
(H) qRT-PCR analysis of PPAR $\delta$  target genes in WAT from *Otud3*<sup>-/-</sup> mice. Data were normalized with *Gapdh* mRNA levels (n = 3 mice for each group). Bars represent mean  $\pm$  SEM. \*\*p < 0.01, \*\*\*p < 0.001 (two-way ANOVA).

(I) Intracellular PPAR $\delta$  ubiquitination assay. PPAR $\delta$  ubiquitination assays were carried out in *Otud3* CRISPR KO HEK293T cells. Cells were transfected with plasmids as indicated. Lysates were immunoprecipitated with anti-FLAG beads and immunoblotted with anti-HA to reveal the ubiquitination levels. The levels of PPAR $\delta$  and OTUD3 were revealed by anti-FLAG and anti-Myc antibodies, respectively.

(J) PPAR $\delta$  ubiquitin chain analysis. HEK293T cells were co-transfected with a PPAR $\delta$  expression vector and the indicated ubiquitin with WT and Lys-48-only plasmids. Whole-cell lysates were prepared and pulled down with anti-FLAG beads; the precipitants were then incubated with purified GST-tagged OTUD3 at 37°C. Immunoblotting with an anti-HA antibody was used to detect ubiquitinated PPAR $\delta$ .

(K) Effect of GW501516 on body weights of HFD-fed *Otud3*<sup>-/-</sup> mice. The HFD-fed *Otud3*<sup>-/-</sup> mice were treated with either vehicle or GW501516 (5 mg/kg/day) for 7 weeks. The body weights were measured every week.

(L and M) Effects of GW501516 on glucose tolerance and insulin sensitivity of HFD-fed *Otud3*<sup>-/-</sup> mice. GTTs (2 g/kg) and ITTs (0.4 U/kg, Humulin-N, Eli Lilly) were performed. Data are expressed as mean  $\pm$  SEM (n = 4), \*p < 0.05, \*\*p < 0.01 between HFD-fed *Otud3*<sup>+/+</sup> and HFD-fed *Otud3*<sup>-/-</sup> mice, #p < 0.05, ##p < 0.01 between HFD-fed *Otud3*<sup>-/-</sup> and HFD-fed *Otud3*<sup>-/-</sup> + GW501516 mice (two-way ANOVA).



lane 3). These results indicate that the overall acetylation levels of OTUD3 are indispensable for its nuclear translocation and for deubiquitylating PPAR $\delta$ .

## DISCUSSION

Here, we report a rare *c.863 G>A* mutation in the *OTUD3* gene in a family with an early age of onset of diabetes. Their MODY-like trait can be manifested in an individual with the heterozygous genotype. To the best of our knowledge, no clinical significance of this mutation has been previously reported. To further confirm whether it appears in other ethnic groups, we have analyzed the association between *OTUD3 c.863 G>A* and diabetes traits using the Type 2 Diabetes Knowledge Portal (<https://t2d.hugeamp.org/variant.html?variant=rs78466831>). We found a positive correlation between chr1:19906459 G>A (rs78466831, corresponding to *OTUD3 c.863 G>A*) with adjusted BMI ( $p = 0.0149$ ,  $\beta = 0.0742$ ,  $n = 21,453$ ) in a dataset of a recent large-scale multiple ethnic GWAS for type 2 diabetes in East Asians (Chen et al., 2021). This finding is consistent with our observation that all the carriers have a history of being overweight (BMI > 25). This result provides further evidence for the association between human *OTUD3* gene mutation and a higher risk of diabetes in a large population of different ethnic groups among East Asians. However, it should be noted that the allele frequency of this mutation was significantly higher in East Asian populations (0.69%) and native Hawaiians (0.18%), while it was almost zero in other populations according to the database of ALFA allele frequency (dbSNP, National Library of Medicine).

OTUD3 was first described as an important factor in the tumorigenesis (Du et al., 2019; Yuan et al., 2015), but its physiological functions are still poorly understood. As DUBs are crucial regulators in diverse signaling pathways (Hu et al., 2013; Hymowitz and Wertz, 2010; Keusekotten et al., 2013), in this study, we used a whole-body *Otud3*<sup>-/-</sup> mice to investigate the potential role of OTUD3 in metabolic diseases. We found that the *Otud3*<sup>-/-</sup>

mice developed worse obesity, dyslipidemia, and insulin resistance than WT mice when challenged with HFD.

The G288 locus of *OTUD3* is conserved between primates and artiodactyl such as human, pig, cattle, and horse. However, it is not conserved between human and mouse. We cannot generate the same mutation in mouse. Since the human *OTUD3* G288D presents an impaired deubiquitinase function, the *Otud3*<sup>-/-</sup> mice can at least demonstrate the important role of OTUD3 in the pathogenesis of obesity and in raising the risk of diabetes. Moreover, as the mutation in humans is heterozygous, we also evaluated the heterozygous *Otud3*<sup>+/-</sup> mice. Overall, the *Otud3*<sup>+/-</sup> mice showed a mixed phenotype between *Otud3*<sup>+/+</sup> and *Otud3*<sup>-/-</sup> mice, and it is more similar to the *Otud3*<sup>+/+</sup> group under ND feeding but more similar to the *Otud3*<sup>-/-</sup> group under HFD challenge.

Since ND-fed *Otud3*<sup>+/-</sup> mice did not present remarkable diabetes traits, it is difficult to understand why the G288D heterozygous carriers in human have a very high risk of diabetes. One possible explanation is that the G288D mutant can exert a dominant-negative effect. We also found that the G288D mutation neither affected the interaction between OTUD3 and its targets nor attenuated its nuclear translocation. The G288D mutant with impaired DUB activity may potentially compete with WT OTUD3 for substrates and decreases the efficiency of WT OTUD3, which also meets the definition of dominant negative (Veitia, 2007). However, further structural and mechanistic studies of G288D mutant are still needed to confirm whether the G288D mutant can exert a dominant-negative effect.

Our result of metabolic cage studies showed no remarkable alteration in energy expenditure, physical activity, or food intake among *Otud3*<sup>+/+</sup>, *Otud3*<sup>+/-</sup>, and *Otud3*<sup>-/-</sup> mice. However, we found significantly higher RER levels in *Otud3*<sup>-/-</sup> mice during the light period. The RER value may predict whether fat or carbohydrate is being utilized as a fuel source as the oxygen content is different between the two substances (Galgani and Ravussin, 2008). In the light period, a decrease in physical activity and food intake leads to a switch in energy metabolism in peripheral

### Figure 6. Glucose or fatty acid overload promotes OTUD3 nuclear translocation and enhances OTUD3 acetylation

- (A) FFAs increased nuclear localization of endogenous OTUD3 in 3T3-L1 cells. 3T3-L1 cells were exposed to oleic acid at indicated concentrations for 8 h. Cytosol and nuclear fractions were prepared and immunoblotted with anti-OTUD3 antibody. The anti-HDAC1 antibody and the anti-tubulin antibody were used to identify the nuclear fraction and cytosolic fraction, respectively.
- (B) Fluorescence microscopy analysis of OTUD3 localization under glucose and FFA overload. HeLa cells were transfected with GFP-tagged OTUD3. Cells were treated with glucose or FFAs for 8 h with indicated concentrations. Nuclei were stained with DAPI. Scale bars, 20  $\mu$ m.
- (C) Effects of glucose and ACLY inhibitor on OTUD3 acetylation in lentivirus-mediated pCDH-FLAG-OTUD3-overexpressing 3T3-L1 stable cell line. Whole-cell extracts were prepared from 3T3-L1 cells incubated in increasing concentrations of glucose as indicated for 24 h; 100  $\mu$ M ACLY inhibitor SB 204990 or vehicle was added into medium as indicated. OTUD3 was purified by anti-FLAG beads. Acetylation levels were revealed by anti-acetyl lysine antibody ( $\alpha$ -Ack).
- (D) Combined effect of glucose and CBP on OTUD3 acetylation. HEK293T cells were transfected with S-HA-OTUD3 and increasing amounts of FLAG-tagged CBP (2, 4, 6, or 8  $\mu$ g plasmid) and then incubated in medium containing 0 or 25 mM glucose for 12 h. Lysates were immunoprecipitated with S-protein beads. Acetylation levels of OTUD3 and total OTUD3 levels were revealed by anti-acetyl lysine and anti-HA antibody, respectively.
- (E) CBP increases nuclear translocation of OTUD3. HEK293T cells were transfected with control plasmid (mock) or FLAG-tagged CBP (CBP). Cytosol and nuclear fractions were prepared and the nuclear translocation of endogenous OTUD3 was revealed by OTUD3 antibody. The anti-HDAC1 antibody and the anti-tubulin antibody were used to identify the nuclear fraction and cytosolic fraction, respectively.
- (F) TSA augments OTUD3 acetylation. 3T3-L1 cells were infected with adenovirus-S-HA-OTUD3. Cells were then incubated with TSA (2  $\mu$ M) or NAM (10 mM) or TSA (2  $\mu$ M) + NAM (10 mM) for 6 h. Whole-cell extracts were prepared and subjected to pull-down assays using S-protein beads. Acetylation levels of OTUD3 and total OTUD3 levels were revealed by anti-acetyl lysine and anti-HA antibody, respectively.
- (G) TSA increases OTUD3 nuclear translocation. 3T3-L1 cells were incubated with TSA (2  $\mu$ M) or NAM (10 mM) alone or TSA (2  $\mu$ M) + NAM (10 mM) for 6 h. Cytosol and nuclear fractions were prepared and immunoblotted with anti-OTUD3 antibody. The anti-HDAC1 antibody and the anti-tubulin antibody were used to identify the nuclear fraction and cytosolic fraction, respectively.
- (H) Schematic illustration of the role of OTUD3 in the regulation of energy metabolism. In response to high glucose or FFA levels, OTUD3 is acetylated by CBP and translocated into the nucleus where it stabilizes various transcriptional factors involved in glucose, lipid metabolism, and oxidative phosphorylation.

**Table 1. Sequences of primers for RT-PCR**

Gene symbol	Forward primer sequence	Reverse primer sequence
Ndufa9 mouse	ACTGTGTTGGGGCTACAGG	GATTGATGACCAGTTGCTG
Sdha mouse	ACACAGACCTGGTGGAGACC	GCACAGTCAGCCTCATTCAA
Uqcrc2 mouse	ATCAAAAGGGGCAACAACAC	CACTCAGGAAGCCCTCTGAC
Cox4 mouse	TTGGCAAGAGAGCCATTCT	GCCACAACCTGTCTCCATT
Atp5a1 mouse	AGGCTATCCTGGTGATGTG	CTTCATGGTACCTGCCACCT
Nd1 mouse	ACGCAAAATCTTAGGGTACA	GAGTGATAGGGTAGGTGCAA
Nd6 mouse	CACCCAGCTACTACCATCAT	ATTGGGGGTGATTATAGAGG
Cox1 mouse	ATTCGAGCAGAATTAGGTCA	CTCCGATTATTAGTGGGACA
Atp6 mouse	ACGAAAATCTATTTGCCCTCA	TGGTGTGTGGATTAGCATT
Ndufa4 mouse	TCCCAGCTTGATTCTCTCTT	GGGTTGTTCTTCTGTCCCAG
Ndufb4 mouse	CGGGTTCCAAGTATAAGCCTG	GTTTGGGGTCTGTACTGAAG
Sdhd mouse	TGGTCAGACCCGCTTATGTG	GAGCAGGGATTCAAGTACCCA
Cox8c mouse	TGCAGTCTGTTCTCGAAGC	GCTGGGATGTAAAAGGTCGTAA
Atp6v1d mouse	GGCAAAGACCGGATTGAAATCT	GTGCAAATCGAAGAGTTAAGGCA
Atp6v1b1 mouse	AAGTTTGCCAGTATGCTGAG	GCAGGATGTCCCCTGTGAA
Atp2a3 mouse	CGTCGCTTCTCGGTGACAG	AAGAGGTCTCAAACCTGCTCC
Actin mouse	CGAGGCCAGAGCAAGAGAG	CGGTTGGCCTTAGGGTTCAG
Dgkk mouse	GAATGAGTCCAGCACTACATCTG	GGACCACGTTATTGGCGGTT
Myo3b mouse	AAAACCGGGAAGCACCTGTAT	GCCTTTGCCAATCGTCTCTATAA
Cyp17a1 mouse	AGTCAAAGACACCTAATGCCAAG	ACGCTCTGGGGAGAAACGGT
Dsc1 mouse	ACACCTGTAGGCAAAGTGAATC	CCTTGACCATCTGAGAGCAAGA
Crisp1 mouse	TGTCCTGTTGGCAATTATCAAGG	CCACAACCTATTGGTGCATAGCC
Scel mouse	GACAACAGGGTTTTGAGGACG	TACCGGCTAATTGTGGCTTTT
Otof mouse	CTGACACGGCATTCTGCTG	CCTGGGAGGCTGTAAAGGAA
Pgap1 mouse	TTCTCCACTCAGTCAACCTCTG	ATGCTGCACCTGTTTTCTCTG
Tox3 mouse	CTGGGGTACTACGGCTACAG	GCGTGTGGAATGTCTGCTCA
Phf19 mouse	ACAGACGGGCTATATTACCTTGG	GATCTCGTTTCATAGGCCCTGA
Ptpro mouse	GCACACTTTTAATTGGACTGCTC	TGCCAGCTCCACATTCCCTA
Dmrta1 mouse	CATCTAAGGGTAATGTGACCGTG	TGGTGGATTTGTCTGGGTGTT
Rab11fip1 mouse	GTTGCTCGGTCTCGATAAGTTC	ACTTCAGGGTGTACCATTGCT
Pax2 mouse	AAGCCCGGAGTGATTGGTG	CAGGCGAACATAGTCGGGTT
Slc38a4 mouse	GCGGGGACAGTATTCAGGAC	GGAACCTCTGACTTTCGGCAT
Grm1 mouse	GAGGCCATGTTCCACACATTA	CCAGCAATAGGCTTCTTAGTCTC
Lipg mouse	ATGCGAAACACGGTTTTCTCTG	GGACGCAAGGTTGTGATACTTC
Ch25h mouse	ATGGGCTGCTACAACGGTTC	CCTTGCTCTTATGGTGTCCCAG
Pdzrn4 mouse	CGGCCAACATACGGCATGA	GGCCATGATGTGTTCAAAGTG
Ndufc2 mouse	GGCCATGAGCCCTTAAAATTCT	CCGTGCAGTAGCCCAACAA
Adiponectin mouse	TCTCC TGTTCTCTT AATCC TGCC	CATCT CCTTT CTCTC CCTTC TCTCC
Cd36 mouse	TGCTG GAGCT GTTAT TGGTG	TGGGT TTTGC ACATC AAAGA
Fasn mouse	CCCTT GATGA AGAGG GATCA	ACTCC ACAGG TGGGA ACAAG
Ucp1 mouse	GTGAACCCGACAACCTCCGAA	TGCCAGGCAAGCTGAAACTC
Ucp3 mouse	CTGCACCGCCAGATGAGTTT	ATCATGGCTTGAAATCGGACC
Aox1 mouse	TCCAGACTTCCAACATGAGGA	CTGGGCGTAGGTGCCAATTA
Lcas mouse	TCCTGACGTTTGGAAACGGC	CTCCCTCAATCCCCACAGAC
Cyp4a12a mouse	CCTCTAATGGCTGCAAGGCTA	CCAGGTGATAGAAGTCCCATCT
Cyp4a30b mouse	TGGATTGGCTACGGTTTGCTC	CACCATGATCCCACATAAGGC
Mmp1a mouse	CCTTGATGAGACGTGGACCAA	ATGTGGTGTGTTGTCACCTGT
Mmp1b mouse	GCTCATGCTTTCTGCCAGG	TAGAATGGGAGAGTCCAAGGG
Abcc8 mouse	CAAGGTGTCTCAACAACGG	CCAGGTGCTATGGTGAATGTG

(Continued on next page)

**Table 1. Continued**

Gene symbol	Forward primer sequence	Reverse primer sequence
Cacna1b mouse	ACAACGTCGTCCGCAAATAC	CAGGGCCAGAACAATGCAGT
Ndufa9 human	GTCACGTTCTGCCATTACTGC	GGTGGTTGACAACATATCGCC
Sdha human	TGAGCCTGTACCGCATCT	GGTTCCTTGGACTGTGC
Uqcr2 human	TTCAGCAATTTAGGAACCACCC	GGTCACACTTAATTTGCCACCAA
Cox4 human	ACTACCCCATGCCAGAAGAG	TCATTGGAGCGACGGTTCATC
Atp5a1 human	GTATTGCCCGCGTACATGG	AGGACATAACCTTTAAGCCTGA
Nd1 human	GTGCAGCATTTACCTTCGC	GAGGTCTCCCACTGTGTTCA
Nd6 human	CAGAGAGACCCATATTCGGGA	GGCTTTTTATTTGGCGCACAA
Cox1 human	GGGCAGCATTCTGTCTCC	CCCAACTGATTTGCACGA
Atp6 human	AAGCAAGGGTTCTCAA	CGGCGCAA
Ndufa4 human	ATGATCGGCTTAATCTGCCTG	TCCGGTGTGTTCTTTCTGTCC
Ndufb4 human	ATGTCGTTCCCAAAGTATAAGCC	GAAGCAGGTA
Sdhd human	ATTTCTTCAGACCGACCTATCC	CAGCCTTGAGCCAGAATG
Atp6v1d human	AGCACAGACAGGTCGAAACC	TTCTCTCATCACTTCGCCCAT
Atp6v1b1 human	GGCGGTCACCCGAAACTAC	GGACGATCTCCGCATACTGG
Atp2a3 human	CTGGTCATCATGCTGATCCTC	CAGCGTGGTGGACTTGATCT
Ndufc2 human	CGGCCTGATTGATAACCTAATCC	AAGCTGGCGATGCAAACCA
Adiponectin human	CTGGATGGTACACGAAGAGGT	TGGGCTTGTAAGAGAGGGGAC
Cd36 human	GGCTGTGACCGAACTGTG	AGGTCTCCA
Fasn human	AAGGACCTGTCTAGGTTTGATGC	TGGTTCATAGGTGACTTCCA
Phf19 human	ACTCGGGACTCCTATGGTGC	CCTCCGTCAGTTTGACATCA
Rab11fp1 human	GCTCGGCCCTCGACAAGTTC	ACTTATACCACTGCGTCTTCTCT
Pax2 human	TGTCAGCAAAATCCTGGGCAG	GTCGGGTTCTGTGTTGTATT
Slc38a4 human	AGAAATTCCAAATACCTGCCCC	GAAGCGTGTGTTGAATGACAG
Grm1 human	CCAGCGATCTTTTGGAGGTG	TGGTGATGGACTGAGAAGAGG
Lipg human	GGGAGCCCCGTACCTTTTG	CCTCACAGATGGTTGACCTCA
Ch25h human	ATCACCACATAGTGGGCTTT	GTCAGGGTGGATCTGTAGCG
Pdzrn4 human	CCAGCACTCAGACGGACATC	CTAACACGACACA
Atp6v1b1 human	GGCGGTCACCCGAAACTAC	GGACGATCTCCGCATACTGG
Ptpro human	CCCAATGTGGTAGTGATCTCCG	AGCTTCCATCCCTCTCTAAGG
Dmrta1 human	GCAGAGACCGAGGCGTTAG	AACCTGCATCCCCGATGGTA
Dgkk human	GAGGCGACCTCAGAATCAGC	GCTCTGGGACCGACTCTAGG
Myo3b human	AGCGGATCACTGTGATGGG	GCCACATCTGAGTAGACCTTTG
Cyp17a1 human	GCTGCTTACCCTAGCTTATTTGT	ACCGAATAGATGGGGCCATATTT
Dsc1 human	AGGCTGAAACACTTGTAGGCA	GTTGTTCCCGTCTCTGACCAT
Crisp1 human	CTTGCTTACTGCCTATGTTGTCC	GGTGGA
Mboat2 human	TTTTGCTTTGGATGGTATGCCT	GCACACTGTGAGGTATCCCA
Scel human	GTGCTCAACCGACATAATTCCC	TGTCATCAGAACTGTACCGACTA
Otof human	CAACAAGCGTGTGCCTATG	TCCTTGCGCTGTTTGCTGA
Pgap1 human	CTTCGGCTTCGAGGAGAATAAG	GGGATAGCGTTTGGCCAGTTT
Tox3 human	ATTCCACCAATCACGCCTCC	GGATCGCTGAGGGCTTGAAA

The table displays gene symbols and forward and reverse sequences of all primers used in this study.

tissues from glucose to FFA oxidation, which is reflected in rapidly falling RER values (Galvani and Ravussin, 2008). In our study, ND-fed *Otud3*-deficient mice showed a higher RER value during the light period, while the physical activity and food intake remained unaffected. That is, this higher RER during light periods does not appear to be related to any changes in food intake,

physical activity, or sleep. These data imply that the animals cannot efficiently switch to FFA oxidation during postprandial phases or during sleep. It also suggests a preference for carbohydrate fuel utilization, and one possible reason for this is a decreased fat oxidation capacity in key metabolic tissues. These data are consistent with our observations that a significant

decrease in OXPHOS subunit expression occurs in isolated mitochondria from major metabolic tissue of *Otud3*<sup>-/-</sup> mice and that there is a decreased OCR in differentiated OTUD3 knockdown 3T3-L1 cells compared with scramble shRNA group. These data are in line with the increased body weight that we have observed in *Otud3*-deficient mice. Possibly due to this deficit in FFA oxidation during the resting state, the KO mice have a tendency to accumulate more fat. However, this deficit in fat oxidation in OTUD3-deficient mice is not very severe, as mice fed an HFD showed no significant differences in VO<sub>2</sub>, VCO<sub>2</sub>, and RER among *Otud3*<sup>+/+</sup>, *Otud3*<sup>+/-</sup>, and *Otud3*<sup>-/-</sup> mice. When lacking carbohydrates as a fuel, OTUD3-deficient mice at least are capable of metabolizing FFAs to meet their energy requirements.

Our results of the metabolic cage reveal a significantly higher RER during the light period in KO mice than WT mice, but the difference in energy expenditure, VO<sub>2</sub>, VCO<sub>2</sub>, and food intake is not significant. It should be noted that the onset of obesity is a long process of fat accumulation. Any slight changes can be accumulated and contribute to the development of obesity. Only a slight change in RER may result in a significant difference in body weight (Kusminski et al., 2020). Also, in contrast to the minimal changes in energy homeostasis, our KO mice showed severe defects in mitochondrial function in adipose tissues and muscle. However, it is worth noting that *ex vivo* assays of mitochondrial function were performed under extreme conditions. The defects in mitochondrial function under physiological conditions may be less severe than what we found *ex vivo*. These observations were consistent with the literature that severe defects in mitochondrial functions only led to a slight change in RER but did not significantly affect the VO<sub>2</sub> and VCO<sub>2</sub> (Kusminski et al., 2020).

As the ND-fed *Otud3*<sup>-/-</sup> mice do not present obesity, glucose intolerance, and insulin resistance, one possible question is whether the glucose intolerance, insulin resistance, and dyslipidemia can be secondary to the obesity phenotype of HFD-fed *Otud3*<sup>-/-</sup> mice. We have studied the major metabolic tissues such as WAT, BAT, skeletal muscle, and liver of *Otud3*<sup>-/-</sup> mice fed either an ND or HFD. We found that all of the tissues were affected by the loss of function of OTUD3 to a certain degree. More importantly, in non-obese and normoglycemic ND-fed *Otud3*<sup>-/-</sup> mice, the mice already present significant alterations in major metabolic tissues, such as increased lipid accumulation in the liver and ectopic lipid disposition in the skeletal muscle, compared with WT mice. These alterations may make the mice predisposed to obesity and other metabolic diseases. Both *Otud3*<sup>-/-</sup> and *Otud3*<sup>+/-</sup> mice develop worse obesity and insulin resistance than WT mice when the groups are all fed an HFD, suggesting a higher risk of diabetes among both groups of mutant mice.

To better understand which tissue is the main functioning tissue of *Otud3* KO accounting for the obesity phenotype, we also evaluated the impact of *Otud3* loss of function on the mitochondrial functions among the major metabolic tissues. We found that the *Otud3* loss of function mainly affected the activity of OXPHOS complexes in visceral adipose tissue. Consistent with this finding, we found a significant decrease in ATP contents in visceral adipose tissue compared with those in WT mice, while the differences in other tissues were non-significant. These results suggest that the visceral adipose tissue might be the

main functioning tissue in energy metabolism accounting for the obese phenotype of *Otud3* KO mice.

The OTUD3 has a strong cytosolic presence: it directly regulates the stability of a variety of cytosolic proteins, including those that are important to insulin action (Yuan et al., 2015). In this study, we discovered that glucose and fatty acid may stimulate the nuclear translocation of OTUD3. Nuclear OTUD3, in turn, promotes glucose and fatty acid metabolism through stabilized diverse energy-metabolism-related transcription factors. OTUD3 has a broad substrate spectrum, and here we have identified a panel of metabolically related transcription factors as substrates of OTUD3. We further discovered that PPAR $\delta$  is one of the key targets. Our rescue experiment showed that the PPAR $\delta$  agonist GW501516 reduced the weight gain and improved glucose tolerance and insulin resistance of HFD-fed *Otud3*<sup>-/-</sup> mice. Moreover, in the literature, GW501516 were reported to slightly reduce body weight (Lefere et al., 2020) and improve glucose tolerance (Tanaka et al., 2003) of HFD-fed WT mice. As the phenotypes of the GW501516-treated *Otud3* KO mice were between vehicle-treated KO and WT mice, the *Otud3* KO mice respond less effectively to PPAR $\delta$  agonist than WT mice. This observation was consistent with the literature because the levels of PPAR $\delta$  protein were significantly reduced in the *Otud3* KO mice. These findings reinforce our hypothesis that PPAR $\delta$  is a key target of OTUD3.

In the literature, PTEN phosphatase has been described to be an important cytosolic target of OTUD3. OTUD3 loss of function increases the Ub-dependent degradation of PTEN and enhances PI3K/AKT signaling in breast cancer cells (Yuan et al., 2015). However, in this study, PTEN does not seem to be the key target in the aspect of energy metabolism according to the phenotype of *Otud3*<sup>-/-</sup> mice. Notably, whole-body *Pten* KO is embryonically lethal in mice (Di Cristofano et al., 1998), while tissue-specific *Pten* deficiency such as in the adipose tissue, pancreas, liver, and muscle is viable, and they present with improved metabolic functions, including increased insulin sensitivity (Kurlawalla-Martinez et al., 2005; Nguyen et al., 2006; Stiles et al., 2004; Tong et al., 2009; Wang et al., 2010,2014; Wijesekara et al., 2005). However, our *Otud3*<sup>-/-</sup> mice developed worse insulin resistance than WT mice did. Furthermore, no significant increase in p-AKT was observed in WAT, muscle, and liver of *Otud3*<sup>-/-</sup> mice under basal condition compared with WT mice. More importantly, we found a decrease in p-AKT levels in WAT, muscle, and liver in *Otud3*<sup>-/-</sup> mice after insulin treatment compared with WT mice. These contradictory findings may be due to the differences between breast cancer cells and normal metabolic tissues.

Since some key adipocyte markers were found to be decreased in the PBMCs of carriers of *OTUD3* c.863 G>A and in adipose tissues of *Otud3*<sup>-/-</sup> mice, one possible question is whether this mutation affects adipocyte differentiation. However, in our opinion, this mutation may not significantly affect adipocyte differentiation as no grossly visible dysplasia of adipose tissues was observed in either ND-fed or HFD-fed *Otud3*<sup>-/-</sup> mice. Also, all the carriers of *OTUD3* c.863 G>A have a history of being overweight. Furthermore, *Otud3*-knockdown 3T3-L1 cells can successfully differentiate into an adipocyte phenotype. However, the differentiated *Otud3*-knockdown 3T3-L1 cells showed several impairments in adipocyte functions such as impaired OXPHOS capacity and lipogenic capacity. These

observations were consistent with the decreased glucose uptake and OCR.

One explanation for this difference in effects is that as OTUD3 is a deubiquitinase, *Otud3* loss of function mainly leads to an increased turnover rate of its targets. It cannot lead to complete degradation of its targets. Therefore, *Otud3*-knockdown 3T3-L1 cells can successfully differentiate into adipocytes, but with some impaired functions. Taken together, these data suggest that OTUD3 loss of function possibly does not affect 3T3-L1 cell differentiation, but rather it mainly affects the metabolic function of differentiated 3T3-L1 cells.

Our study reveals that the nuclear translocation of OTUD3 require its acetylation. Multiple acetylation sites were identified in OTUD3, but none of the single-substituted lysine mutants exhibited lower levels of overall acetylation. However, its DUB activity is reported to depend mainly on the acetylation of Lys129 (Zhang et al., 2020). We further demonstrated that the CBP acetyltransferase, a crucial cofactor in the regulation of energy homeostasis through its acetyltransferase activity, regulates the acetylation and translocation of OTUD3. This finding implies a potential link between the glucose and lipid sensing system and the OTUD3 translocation. An overload of glucose or fatty acids results in an increase in acetyl-CoA levels and facilitates the action of acetyltransferase (Wellen et al., 2009). High glucose levels also increase the acetylation levels of CBP and promote its activity; this result is coherent with a previous study (Cordero-Herrera et al., 2017). Moreover, CBP can be phosphorylated by Akt, which increases its acetyltransferase activity (Liu et al., 2013). Additionally, we found that high glucose levels increase the interaction between OTUD3 and CBP. These data suggest that CBP is one of the key mediators, which establishes the link between glucose sensing and OTUD3 signaling. The activation of CBP by Akt also suggests that the CBP-OTUD3 pathway may be an important mechanism of insulin signaling.

However, it should be noted that no evidence showed that OTUD3 G288D mutant is associated with altered acetylation levels. Also, no evidence showed that G288D affects the nuclear translocation of OTUD3. The G288D mutation mainly affects its stability and DUB enzyme activity, although the CBP-dependent nuclear translocation of OTUD3 may not completely explain the obese phenotype and higher risk of diabetes in carriers of *OTUD3* c.863 G>A mutation. Nevertheless, it represents an important regulation mechanism of energy metabolism as it may stabilize the numbers of transcription factors related to energy metabolism in response to the nutrition signal.

### Conclusions

In summary, we demonstrated that the CBP-dependent OTUD3 nuclear translocation stabilizes various cofactors involved in glucose and lipid metabolism and OXPHOS. This signaling pathway may be a novel regulation mechanism for glucose and fatty acid metabolism. We also identify a rare mutation c.863.G>A in *OTUD3* gene in a family with an early age of onset of diabetes; this mutation is associated with obesity and a higher risk of diabetes. These findings will broaden the current appreciation of the role of OTUD3 and thus help us better understand the pathophysiology of glucose and lipid metabolism regulation.

### Limitations of study

This study also has some limitations. First, we used *Otud3*<sup>-/-</sup> mice model to study the metabolic function of OTUD3 and its potential role in the pathogenesis of diabetes. However, we have not evaluated the effect of OTUD3 overexpression in this study. Yuan et al. have studied OTUD3 overexpression in mice in their study on the role of OTUD3 in tumorigenesis (Yuan et al., 2015). They found that *Otud3* transgenic mice showed a decreased body size. Whether OTUD3 overexpression ameliorates diabetes and/or obesity needs further exploration. Also, to what extent *Otud3*<sup>-/-</sup> mice mimic human c.863G>A (G288D) mutation still needs further investigations. However, as this segment of sequence is not conserved between human and mouse, we were unable to construct an identical mutation in mice by gene editing. Whether there are other mechanisms besides decreased stability and activity needs further investigation. Moreover, we have not determined which mechanism, among reduced stability, impaired DUB activity, and dominant-negative effect, was the major mechanism of the G288D mutant of OTUD3. Finally, it is still not fully clear in which tissue(s) OTUD3 primarily exerts its function in controlling energy metabolism. To better understand the main functioning tissues accounting for the obese phenotype and high risk of diabetes, conditional KO animals are needed in future studies to better determine this level of control.

### STAR★METHODS

Detailed methods are provided in the online version of this paper and include the following:

- KEY RESOURCES TABLE
- RESOURCE AVAILABILITY
  - Lead contact
  - Materials availability
  - Data and code availability
- EXPERIMENTAL MODEL AND SUBJECT DETAILS
  - Human blood specimen collection
  - Mouse model
  - Housing conditions of experimental animals
  - Mouse dietary regimen
  - Cell culture, plasmid generation and transfection
- METHOD DETAILS
  - Whole exome sequencing
  - Lentivirus packaging and infection (pCDH-CMV-MCS-EF1-Puro lentiviral system)
  - Lentivirus packaging and infection (pLKO.1-TRC lentiviral shRNA system)
  - Lentivirus packaging and infection (lentiCRISPR v2 system) in OTUD3 knockout stable cell line of HEK293T and 3T3-L1
  - Intraperitoneal glucose and insulin tolerance tests
  - Serum insulin and lipid measurements
  - PPAR $\delta$  agonist GW501516 treatment
  - Immunohistochemistry
  - Oil Red O Staining
  - ATP content
  - Mitochondria Isolation
  - Mitochondrial Electron Transport Chain Complex Activity Assays

- Blue native PAGE (BN-PAGE) and blotting
- Lactate measurement
- Glucose uptake assay
- Targeted metabolomics quantification by LC-MS
- Measurement of oxygen consumption rate
- Quantitative RT-PCR
- S-tag pulldown, Flag pulldown and Mass spectrometry analysis
- Confocal microscopy
- Co-immunoprecipitation assay (Co-IP)
- Chromatin-immunoprecipitation sequencing (ChIP-seq)
- Cytoplasmic and nuclear fractions preparation
- RNA-seq procedures
- OTUD3 protein purification
- Ubiquitinated protein purification
- Deubiquitination assay for ubiquitinated protein
- Metabolic cage
- **QUANTIFICATION AND STATISTICAL ANALYSIS**

#### SUPPLEMENTAL INFORMATION

Supplemental information can be found online at <https://doi.org/10.1016/j.cmet.2022.05.005>.

#### ACKNOWLEDGMENTS

We thank the National Center for Protein Sciences at Peking University in Beijing, China, for assistance with XF Extracellular Flux Analyzer. We thank Y. Yuan and X. Zhao for mass spectrometry analysis. We thank L. Liang for computational analysis of the protein structure of OTUD3 and X. Chen and C.Q. Liu for assistance with animal procedures and experiments. We thank G. Li for help with the initial stages of the project, X. Li for assistance with human genetic studies, and H. Liang and L. Yuan for technical assistance and critical discussion. We thank M. He for the graphical abstract (created with [BioRender.com](https://BioRender.com), #EJ23W7VD37). This work was supported by grants to Y.Y., including the National Natural Science Foundation of China (key grants #82030081 and #81874235), the National Key Research and Development Program of China (grant #2021YFA1300601) and the Lam Chung Nin Foundation for Systems Biomedicine. It was also supported by grants to Y.S. from the National Natural Science Foundation of China (grants #81922016 and #81870607) and Natural Science Foundation of Shandong Province of China (grants #ZR2019JQ25 and #ZR2020ZD14).

#### AUTHOR CONTRIBUTIONS

Y.Y. conceived the project. Y.S., N.Z., H.Q., and Junjun Liu contributed to the study design, data acquisition, analysis, and figure preparation. N.Z., H.Q., and N.L. performed some animal experiments. G.Z., Z.Z., and X.B. performed bioinformatics analysis. X.Z. performed mass spectrometry analysis. C.S., M.Z., and J.G. established *Otud3* knockout mice. N.Z. provided clinical blood samples of individuals with diabetes. Jianping Liu was in charge of communicating with individuals with diabetes. R.L. guided chemical use. The manuscript was written by N.Z., H.Q., Junjun Liu, Y.S., and Y.Y.

#### DECLARATION OF INTERESTS

The authors declare no competing interests.

Received: January 31, 2021

Revised: March 1, 2022

Accepted: May 16, 2022

Published: June 7, 2022

#### REFERENCES

- Abdul Rehman, S.A., Kristariyanto, Y.A., Choi, S.Y., Nkosi, P.J., Weidlich, S., Labib, K., Hofmann, K., and Kulathu, Y. (2016). MINDY-1 is a member of an evolutionarily conserved and structurally distinct new family of deubiquitinating enzymes. *Mol. Cell* 63, 146–155.
- Arda, H.E., Li, L., Tsai, J., Torre, E.A., Rosli, Y., Peiris, H., Spitale, R.C., Dai, C., Gu, X., Qu, K., et al. (2016). Age-dependent pancreatic gene regulation reveals mechanisms governing human beta cell function. *Cell Metab.* 23, 909–920.
- Bastidas-Ponce, A., Roscioni, S.S., Burtscher, I., Bader, E., Sterr, M., Bakhti, M., and Lickert, H. (2017). Foxa2 and Pdx1 cooperatively regulate postnatal maturation of pancreatic beta-cells. *Mol. Metab.* 6, 524–534.
- Chen, J., Spracklen, C.N., Marenne, G., Varshney, A., Corbin, L.J., Luan, J., Willems, S.M., Wu, Y., Zhang, X., Horikoshi, M., et al. (2021). The trans-ancestral genomic architecture of glycemic traits. *Nat. Genet.* 53, 840–860.
- Clague, M.J., Coulson, J.M., and Urbé, S. (2012). Cellular functions of the DUBs. *J. Cell Sci.* 125, 277–286.
- Clague, M.J., Barsukov, I., Coulson, J.M., Liu, H., Rigden, D.J., and Urbé, S. (2013). Deubiquitylases from genes to organism. *Physiol. Rev.* 93, 1289–1315.
- Cordero-Herrera, I., Chen, X., Ramos, S., and Devaraj, S. (2017). (–)-Epicatechin attenuates high-glucose-induced inflammation by epigenetic modulation in human monocytes. *Eur. J. Nutr.* 56, 1369–1373.
- Dancy, B.M., and Cole, P.A. (2015). Protein lysine acetylation by p300/CBP. *Chem. Rev.* 115, 2419–2452.
- DeFronzo, R.A., Bonadonna, R.C., and Ferrannini, E. (1992). Pathogenesis of NIDDM. A balanced overview. *Diabetes Care* 15, 318–368.
- Di Cristofano, A., Pesce, B., Cordon-Cardo, C., and Pandolfi, P.P. (1998). Pten is essential for embryonic development and tumour suppression. *Nat. Genet.* 19, 348–355.
- Du, T., Li, H., Fan, Y., Yuan, L., Guo, X., Zhu, Q., Yao, Y., Li, X., Liu, C., Yu, X., et al. (2019). The deubiquitylase OTUD3 stabilizes GRP78 and promotes lung tumorigenesis. *Nat. Commun.* 10, 2914.
- Dubois-Laforgue, D., Cornu, E., Saint-Martin, C., Coste, J., Bellanné-Chantelot, C., and Timsit, J.; Monogenic Diabetes Study Group of the Societe Francophone du Diabète (2017). Diabetes, associated clinical spectrum, long-term prognosis, and genotype/phenotype correlations in 201 adult patients with hepatocyte nuclear factor 1B (HNF1B) molecular defects. *Diabetes Care* 40, 1436–1443.
- Ellard, S., Lango Allen, H., De Franco, E., Flanagan, S.E., Hysenaj, G., Colclough, K., Houghton, J.A., Shepherd, M., Hattersley, A.T., Weedon, M.N., and Caswell, R. (2013). Improved genetic testing for monogenic diabetes using targeted next-generation sequencing. *Diabetologia* 56, 1958–1963.
- Galgani, J., and Ravussin, E. (2008). Energy metabolism, fuel selection and body weight regulation. *Int. J. Obes. (Lond)* 32 (Suppl 7), S109–S119.
- Hu, H., Brittain, G.C., Chang, J.H., Puebla-Osorio, N., Jin, J., Zal, A., Xiao, Y., Cheng, X., Chang, M., Fu, Y.X., et al. (2013). OTUD7B controls non-canonical NF- $\kappa$ B activation through deubiquitination of TRAF3. *Nature* 494, 371–374.
- Huang, W., Liu, X., Queen, N.J., and Cao, L. (2017). Targeting visceral fat by intraperitoneal delivery of novel AAV serotype vector restricting off-target transduction in liver. *Mol. Ther. Methods Clin. Dev.* 6, 68–78.
- Hymowitz, S.G., and Wertz, I.E. (2010). A20: from ubiquitin editing to tumour suppression. *Nat. Rev. Cancer* 10, 332–341.
- Itani, S.I., Zhou, Q., Pories, W.J., MacDonald, K.G., and Dohm, G.L. (2000). Involvement of protein kinase C in human skeletal muscle insulin resistance and obesity. *Diabetes* 49, 1353–1358.
- Karastergiou, K., Fried, S.K., Xie, H., Lee, M.J., Divoux, A., Rosencrantz, M.A., Chang, R.J., and Smith, S.R. (2013). Distinct developmental signatures of human abdominal and gluteal subcutaneous adipose tissue depots. *J. Clin. Endocrinol. Metab.* 98, 362–371.
- Keenan, A.B., Torre, D., Lachmann, A., Leong, A.K., Wojciechowicz, M.L., Utti, V., Jagodnik, K.M., Kropiwnicki, E., Wang, Z., and Ma'ayan, A. (2019). ChEA3: transcription factor enrichment analysis by orthogonal omics integration. *Nucleic Acids Res.* 47, W212–W224.
- Keusekotten, K., Elliott, P.R., Glockner, L., Fill, B.K., Damgaard, R.B., Kulathu, Y., Wauer, T., Hospenthal, M.K., Gyrd-Hansen, M., Krappmann, D., et al.

(2013). OTULIN antagonizes LUBAC signaling by specifically hydrolyzing Met1-linked polyubiquitin. *Cell* 153, 1312–1326.

Komander, D., Clague, M.J., and Urbé, S. (2009). Breaking the chains: structure and function of the deubiquitinases. *Nat. Rev. Mol. Cell Biol.* 10, 550–563.

Konvalova, S. (2019). Analysis of mitochondrial respiratory chain complexes in cultured human cells using blue native polyacrylamide gel electrophoresis and immunoblotting. *J. Vis. Exp.* e59269.

Kurlawalla-Martinez, C., Stiles, B., Wang, Y., Devaskar, S.U., Kahn, B.B., and Wu, H. (2005). Insulin hypersensitivity and resistance to streptozotocin-induced diabetes in mice lacking PTEN in adipose tissue. *Mol. Cell. Biol.* 25, 2498–2510.

Kuschnerus, K., Straessler, E.T., Müller, M.F., Lüscher, T.F., Landmesser, U., and Kränkel, N. (2019). Increased expression of miR-483-3p impairs the vascular response to injury in type 2 diabetes. *Diabetes* 68, 349–360.

Kusminski, C.M., Ghaben, A.L., Morley, T.S., Samms, R.J., Adams, A.C., An, Y., Johnson, J.A., Joffin, N., Onodera, T., Crewe, C., et al. (2020). A novel model of diabetic complications: adipocyte mitochondrial dysfunction triggers massive beta-cell hyperplasia. *Diabetes* 69, 313–330.

Lee, A.V., Gooch, J.L., Oesterreich, S., Guler, R.L., and Yee, D. (2000). Insulin-like growth factor I-induced degradation of insulin receptor substrate 1 is mediated by the 26S proteasome and blocked by phosphatidylinositol 3'-kinase inhibition. *Mol. Cell. Biol.* 20, 1489–1496.

Lefere, S., Puengel, T., Hundertmark, J., Penners, C., Frank, A.K., Guillot, A., de Muynck, K., Heymann, F., Adarbes, V., Defrêne, E., et al. (2020). Differential effects of selective- and pan-PPAR agonists on experimental steatohepatitis and hepatic macrophages<sup>\*</sup>. *J. Hepatol.* 73, 757–770.

Liu, Y., Xing, Z.B., Zhang, J.H., and Fang, Y. (2013). Akt kinase targets the association of CBP with histone H3 to regulate the acetylation of lysine K18. *FEBS Lett.* 587, 847–853.

Liu, J., Lian, G., Wang, T., Ma, Y., Zhou, J., Jiang, C., and Yin, Y. (2017). An HPLC-MS/MS method for quantitation of Gly-MCA in mouse plasma: application to a pharmacokinetic study. *J. Pharm. Biomed. Anal.* 146, 53–58.

Manickam, R., and Wahli, W. (2017). Roles of peroxisome proliferator-activated receptor  $\beta/\delta$  in skeletal muscle physiology. *Biochimie* 136, 42–48.

Melkman-Zehavi, T., Oren, R., Kredon-Russo, S., Shapira, T., Mandelbaum, A.D., Rivkin, N., Nir, T., Lennox, K.A., Behlke, M.A., Dor, Y., and Hornstein, E. (2011). miRNAs control insulin content in pancreatic beta-cells via downregulation of transcriptional repressors. *EMBO J.* 30, 835–845.

Mohan, V., Pranjali, P.P., Amutha, A., Ganesan, A., Datta, M., and Gayathri, P. (2009). Prevalence and clinical profile of autosomal dominant type 2 diabetes from a diabetes centre in India. *Prim. Care Diabetes* 3, 233–238.

Mohlke, K.L., and Boehnke, M. (2015). Recent advances in understanding the genetic architecture of type 2 diabetes. *Hum. Mol. Genet.* 24, R85–R92.

Nguyen, K.T., Tajmir, P., Lin, C.H., Liadis, N., Zhu, X.D., Eweida, M., Tolasa-Karaman, G., Cai, F., Wang, R., Kitamura, T., et al. (2006). Essential role of Pten in body size determination and pancreatic beta-cell homeostasis in vivo. *Mol. Cell. Biol.* 26, 4511–4518.

Nijman, S.M., Luna-Vargas, M.P., Velds, A., Brummelkamp, T.R., Dirac, A.M., Sixma, T.K., and Bernards, R. (2005). A genomic and functional inventory of deubiquitinating enzymes. *Cell* 123, 773–786.

Qi, L., Heredia, J.E., Altarejos, J.Y., Screenshot, R., Goebel, N., Niessen, S., Macleod, I.X., Liew, C.W., Kulkarni, R.N., Bain, J., et al. (2006). TRB3 links the E3 ubiquitin ligase COP1 to lipid metabolism. *Science* 312, 1763–1766.

Qi, J., Gong, J., Zhao, T., Zhao, J., Lam, P., Ye, J., Li, J.Z., Wu, J., Zhou, H.M., and Li, P. (2008). Downregulation of AMP-activated protein kinase by Cidea-

mediated ubiquitination and degradation in brown adipose tissue. *EMBO J.* 27, 1537–1548.

Reyes-Turcu, F.E., Ventii, K.H., and Wilkinson, K.D. (2009). Regulation and cellular roles of ubiquitin-specific deubiquitinating enzymes. *Annu. Rev. Biochem.* 78, 363–397.

Stiles, B., Wang, Y., Stahl, A., Bassilian, S., Lee, W.P., Kim, Y.J., Sherwin, R., Devaskar, S., Lesche, R., Magnuson, M.A., and Wu, H. (2004). Liver-specific deletion of negative regulator Pten results in fatty liver and insulin hypersensitivity [corrected]. *Proc. Natl. Acad. Sci. USA* 101, 2082–2087.

Tanaka, T., Yamamoto, J., Iwasaki, S., Asaba, H., Hamura, H., Ikeda, Y., Watanabe, M., Magoori, K., Ioka, R.X., Tachibana, K., et al. (2003). Activation of peroxisome proliferator-activated receptor delta induces fatty acid beta-oxidation in skeletal muscle and attenuates metabolic syndrome. *Proc. Natl. Acad. Sci. USA* 100, 15924–15929.

Tong, Z., Fan, Y., Zhang, W., Xu, J., Cheng, J., Ding, M., and Deng, H. (2009). Pancreas-specific Pten deficiency causes partial resistance to diabetes and elevated hepatic AKT signaling. *Cell Res.* 19, 710–719.

Vecchione, A., Marchese, A., Henry, P., Rotin, D., and Morriore, A. (2003). The Grb10/Nedd4 complex regulates ligand-induced ubiquitination and stability of the insulin-like growth factor I receptor. *Mol. Cell. Biol.* 23, 3363–3372.

Veitia, R.A. (2007). Exploring the molecular etiology of dominant-negative mutations. *Plant Cell* 19, 3843–3851.

Wang, Y.X., Lee, C.H., Tjep, S., Yu, R.T., Ham, J., Kang, H., and Evans, R.M. (2003). Peroxisome-proliferator-activated receptor delta activates fat metabolism to prevent obesity. *Cell* 113, 159–170.

Wang, L., Liu, Y., Yan Lu, S., Nguyen, K.T., Schroer, S.A., Suzuki, A., Mak, T.W., Gaisano, H., and Woo, M. (2010). Deletion of Pten in pancreatic  $\beta$ -cells protects against deficient  $\beta$ -cell mass and function in mouse models of type 2 diabetes. *Diabetes* 59, 3117–3126.

Wang, L., Opland, D., Tsai, S., Luk, C.T., Schroer, S.A., Allison, M.B., Elia, A.J., Furlonger, C., Suzuki, A., Paige, C.J., et al. (2014). Pten deletion in RIP-Cre neurons protects against type 2 diabetes by activating the anti-inflammatory reflex. *Nat. Med.* 20, 484–492.

Wellen, K.E., Hatzivassiliou, G., Sachdeva, U.M., Bui, T.V., Cross, J.R., and Thompson, C.B. (2009). ATP-citrate lyase links cellular metabolism to histone acetylation. *Science* 324, 1076–1080.

Wijesekara, N., Konrad, D., Eweida, M., Jefferies, C., Liadis, N., Giacca, A., Crackower, M., Suzuki, A., Mak, T.W., Kahn, C.R., et al. (2005). Muscle-specific Pten deletion protects against insulin resistance and diabetes. *Mol. Cell. Biol.* 25, 1135–1145.

Xu, X., Sarikas, A., Dias-Santagata, D.C., Dolios, G., Lafontant, P.J., Tsai, S.C., Zhu, W., Nakajima, H., Nakajima, H.O., Field, L.J., et al. (2008). The CUL7 E3 ubiquitin ligase targets insulin receptor substrate 1 for ubiquitin-dependent degradation. *Mol. Cell* 30, 403–414.

Yuan, L., Lv, Y., Li, H., Gao, H., Song, S., Zhang, Y., Xing, G., Kong, X., Wang, L., Li, Y., et al. (2015). Deubiquitylase OTUD3 regulates PTEN stability and suppresses tumorigenesis. *Nat. Cell Biol.* 17, 1169–1181.

Zhang, Z., Fang, X., Wu, X., Ling, L., Chu, F., Li, J., Wang, S., Zang, J., Zhang, B., Ye, S., et al. (2020). Acetylation-dependent deubiquitinase OTUD3 controls MAVS activation in innate antiviral immunity. *Mol. Cell* 79, 304–319.e7.

Zheng, Y., Ley, S.H., and Hu, F.B. (2018). Global aetiology and epidemiology of type 2 diabetes mellitus and its complications. *Nat. Rev. Endocrinol.* 14, 88–98.

Zhou, J., and Yin, Y. (2016). Strategies for large-scale targeted metabolomics quantification by liquid chromatography-mass spectrometry. *Analyst* 141, 6362–6373.

STAR★METHODS

KEY RESOURCES TABLE

REAGENT or RESOURCE	SOURCE	IDENTIFIER
<b>Antibodies</b>		
Anti-PPAR $\delta$	Abcam	ab23673; RRID:AB_2165902
Anti-FOXN1	Abcam	ab113235; RRID:AB_10865755
Anti-FOXA2	Abcam	ab256493
Anti-HNF1 $\beta$	Abcam	ab128912; RRID:AB_11142227
Anti-PPAR $\gamma$	Abcam	ab178860
Anti-SIX3	Abcam	ab172131
Anti-NDUFB8	Abcam	ab192878; RRID:AB_2847808
Anti-SDHA	Abcam	ab137040; RRID:AB_2884996
Anti-UQCRC2	Abcam	ab203832; RRID:AB_2797139
Anti-COX4	Abcam	ab202554; RRID:AB_2861351
Anti-ATP5A	Abcam	ab176569; RRID:AB_2801536
Anti-GAPDH	Abcam	ab181602; RRID:AB_2630358
Anti-Myc	Abcam	ab32; RRID:AB_303599
Anti-pan-acetyl lysine Antibody	Abcam	ab21623; RRID:AB_446436
Anti-HA antibody	CST	3724; RRID:AB_1549585
Anti-Akt (pan) (C67E7)	CST	4691; RRID:AB_915783
Anti-Akt (pan) (11E7)	CST	4685; RRID:AB_2225340
Anti-Phospho-Akt (Ser473) (D9E)	CST	4060; RRID:AB_2315049
ChIP garde anti-Flag antibody	CST	14793; RRID:AB_2572291
Anti-pan-acetyl lysine Antibody	CST	9441; RRID:AB_331805
Anti-HDAC1	CST	34589; RRID:AB_2756821
Anti-OTUD3	Sigma-Aldrich	HPA028543; RRID:AB_10599302
Anti-Flag M2 antibody	Sigma-Aldrich	F3165; RRID:AB_259529
Anti-Flag M2 Affinity Gel	Sigma-Aldrich	A2220; RRID:AB_10063035
Rabbit anti-Flag antibody	Sigma-Aldrich	F7425; RRID:AB_439687
Anti-HA antibody	Sigma-Aldrich	H3663; RRID:AB_262051
S-protein Agarose	Merck Millipore	69704-4
Anti-Myc	Santa Cruz	sc-40; RRID:AB_627268
Anti-PPAR $\beta/\delta$	Santa Cruz	sc-7197; RRID:AB_2268420
Anti-HOXB8	Abnova	H00003218-M01A; RRID:AB_1237735
Anti-BHLHE22	Proteintech	25622-1-AP; RRID:AB_2880165
Anti- $\beta$ -Actin	MBL	PM053; RRID:AB_10598196
Anti- $\alpha$ -Tubulin	EasyBio	BE0026-100
<b>Chemicals, peptides, and recombinant proteins</b>		
MG132	Sigma-Aldrich	474790
Trichostatin A (TSA)	Sigma-Aldrich	V900931
Nicotinamide (NAM)	Sigma-Aldrich	N0636
Polybrene	Sigma-Aldrich	TR-1003
Polyethylenimine	Sigma-Aldrich	408727
Oleic acid	Sigma-Aldrich	O1383
Palmitate	Sigma-Aldrich	P0500
Fatty-acid free BSA	Sigma-Aldrich	SRE0098
Cellytic MT	Sigma-Aldrich	C3228
Cycloheximide (CHX)	Selleck	S7418

(Continued on next page)

**Continued**

REAGENT or RESOURCE	SOURCE	IDENTIFIER
Acetyl-CoA	Solarbio	A8070
Lipofectamine 3000	Invitrogen	L3000-015
TransIntro EL Transfection Reagent	Transgen	FT201
GW501516	Enzo Life Sciences	ALX-420-032
Insulin (Humulin-N)	Eli Lilly	N/A
Insulin (Regular insulin)	Wanbang	N/A

**Critical commercial assays**

Insulin Mouse Ultrasensitive ELISA kit	ALPCO	80-INSMSU-E01
Mouse free cholesterol ELISA kit	Applygen	E1005
Mouse total cholesterol ELISA kit	Applygen	E1006
Serum NEFA kit	WAKO	294-63601
Triglyceride assay kit	LabAssay	290-63701
ATP Bioluminescence Assay Kit HS II	Roche	11699709001
Mitochondrial respiratory chain complex I Activity Assay Kit	Solarbio	BC0510
Mitochondrial respiratory chain complex II Activity Assay Kit	Solarbio	BC3230
Cytochrome C Mitochondrial respiratory chain complex III activity assay kit	Solarbio	BC3245
Mitochondrial respiratory chain complex IV activity assay kit	Solarbio	BC0945
Mitochondrial respiratory chain complex V activity assay kit	Solarbio	BC1445
L-lactate assay kit	Sigma-Aldrich	MAK065
Glucose uptake colorimetric assay kit	Sigma-Aldrich	MAK083
Seahorse XF Mito stress test kit	Agilent	103015-100
Seahorse XF Glycolytic rate assay kit	Agilent	103020-100
QuikChange II XL Site-Directed Mutagenesis Kit	Stratagene	#200521
ChIP Assay Kit	Millipore	17-371

**Deposited data**

RNA-seq data of adipose tissues of WT and <i>Outd3</i> KO mice	This paper	GEO: GSE201509
ChIP-seq data of mice adipose tissues	This paper	GEO: GSE201430
Source data related to <a href="#">Figures 1, 2, 3, 4, 5, 6, and S1–S7</a>	This paper	<a href="#">Data S1</a>

**Experimental models: Cell lines**

HEK293T	ATCC	CRL-11268
3T3-L1	ATCC	CL-173
HeLa	ATCC	CCL-2

**Experimental models: Organisms/strains**

<i>Outd3</i> KO mouse	This paper	N/A
Oligonucleotides		
Primers for RT PCR	This paper	<a href="#">Table 1</a>

**Recombinant DNA**

pCDH-CMV-MCS-EF1-Puro	System Biosciences	CD510B-1
pCMV-3Tag-3A	Agilent	#240195
pCMV-3Tag-3B	Agilent	#240196
pET28a	EMD Biosciences	#69864-3
pGEX-4T-1	Amersham	#27-4580-01
pADM-CMV-Flag	Vigenebio	N/A
pAV-CMV-3*Flag-GFP	Vigenebio	N/A

(Continued on next page)

**Continued**

REAGENT or RESOURCE	SOURCE	IDENTIFIER
pLKO.1-TRC	Addgene	#85208
lentiCRISPR v2	Addgene	#52961
<b>Software and algorithms</b>		
GraphPad Prism	GraphPad Software	<a href="https://www.graphpad.com">https://www.graphpad.com</a>
R	The R Project	<a href="https://www.r-project.org/">https://www.r-project.org/</a>
edgeR	edgeR package	<a href="https://bioconductor.org/packages/release/bioc/html/edgeR.html">https://bioconductor.org/packages/release/bioc/html/edgeR.html</a>
<b>Other</b>		
Normal diet	Research Diets	D10001
High fat diet	Research Diets	D12492

**RESOURCE AVAILABILITY**

**Lead contact**

Further information and requests for resources and reagents should be directed to and will be fulfilled by the lead contact, Yuxin Yin ([yinyuxin@bjmu.edu.cn](mailto:yinyuxin@bjmu.edu.cn)).

**Materials availability**

*Otud3* KO mouse strains and *Otud3* plasmids generated in this study are available from the lead contact upon reasonable request. This study did not generate new unique reagents.

**Data and code availability**

- RNA-seq data and ChIP-seq data have been deposited at GEO. Data are publicly available as of the date of publication and accession numbers are listed in the [key resources table](#). Uncropped scans of all Western blots and all raw data related to [Figures 1, 2, 3, 4, 5, 6](#), and [S1–S7](#) can be found in [Data S1 – Source Data](#).
- This paper does not report original code.
- Any additional information required to reanalyze the data reported in this paper is available from the lead contact upon request.

**EXPERIMENTAL MODEL AND SUBJECT DETAILS**

**Human blood specimen collection**

Human blood specimens were collected at multiple centers by qualified medical staffs. A total of 316 individuals with diabetes and 313 controls without diabetes were enrolled according to the diagnostic criteria for diabetes mellitus without any age or gender preference. We have excluded individuals with known blood transmitted infectious diseases, chronic inflammatory systemic diseases and other significant disease e.g., severe cardiac, liver, kidney disease or tumors.

Information obtained from all subjects and/or their relatives prior to sample collection were kept confidential. Informed consents were obtained from all subjects and that the experiments conformed to the principles set out in the WMA Declaration of Helsinki and the Department of Health and Human Services Belmont Report. All procedures were approved by the Ethics Committee for the Investigation of Human Subjects in the Peking University Health Science Center. For sequencing analysis, genomic DNA was extracted from blood samples using the TIANamp Blood DNA kit (TIANGEN) and then used as templates for PCR amplification of the functional exons of OTUD3. The products of amplifications were subject to sequencing and results were analyzed with Vector NTI software.

**Mouse model**

All animal experiments procedures were executed in accordance with the Peking University Health Guide for the Care and Use of Laboratory Animal. This study was approved by the Biological Research Ethics Committee of Peking University (project license number: LA2019115).

*Otud3*<sup>-/-</sup> mice were constructed by using the CRISPR/Cas9 system. Cas9 mRNA and sgRNA (5'-GACCAGTTGGAGGGCCACTCT-3') were generated by mMACHINE T7 ULTRA Transcription Kit (AM1345; Thermo Fisher), and MEGAshortscript T7 Transcription Kit (AM1354; Thermo Fisher) respectively, and then injected into zygotes from C57BL/6 mice, followed by transplantation into pseudopregnant ICR mice. The off-springs were genotyped and sequenced by PCR primers with the following sequences: 5'-GGGAGTTTAAGGCCTTAGGCCTGGAGTG-3' and 5'-CTGGGAGGTGGTGGTGTGTGTGAGG-3'. Two founders were obtained. *Otud3*<sup>-/-</sup> mice were back crossed with C57BL/6 for 8 generations before being used in order to minimize the off-target effect of the CRISPR/Cas9 system.

### Housing conditions of experimental animals

Mice were bred and housed in a special pathogen-free facility maintained in a 12/12 h light/dark cycle at a temperature of 20–24 °C with 40%–70% humidity. Maximal 5 mice from same litter were housed in a cage and had free access to water and food. *Otud3*<sup>+/-</sup> mice were mated to produce the *Otud3*<sup>+/+</sup>, *Otud3*<sup>+/-</sup> and *Otud3*<sup>-/-</sup> offspring. We have not differentially housed the pups according to their genotype. Pups with different genotypes from the same litter were kept in the same cage to ensure the three genotypes of mice were maintained in the same environment. Each mouse is assigned a unique identification number and the experimenters do not know their genotypes until the end of the experiment. For metabolic analysis, each mouse was housed individually in metabolic cage during 7 days experiment.

### Mouse dietary regimen

8 weeks old *Otud3*<sup>-/-</sup>, *Otud3*<sup>+/-</sup> and wild-type male mice with an enriched C57BL/6 background were randomly assigned to six groups. They were fed a normal diet (ND) with 4% (w/w) fat content (D10001, Research Diets, New Brunswick, NJ) or a high fat diet (HFD) (D12492, Research Diets, New Brunswick, NJ) (60% kcal from fat) for 10 weeks. Mice with different genotypes from the same litter were kept in the same cage to receive ND or HFD to ensure they were maintained in the same environment.

### Cell culture, plasmid generation and transfection

Cell lines HEK293T (ATCC, CRL-11268) and 3T3-L1 (ATCC, CL-173) were obtained from the American Type Culture Collection. Cells were cultured in DMEM supplemented with 10% (vol/vol) FBS or NBS for 3T3-L1 at 37 °C in a humidified 5% CO<sub>2</sub> atmosphere (Thermo). OTUD3 plasmid was generated by sub-cloning human OTUD3 cDNA (including full-length or various truncations) into pCMV-3Tag-3A (Agilent Technologies, pCMV-3Tag-3A/3B, Catalog #240195), pCMV-3Tag-3B (Agilent Technologies, pCMV-3Tag-3A/3B, Catalog #240196), S-HA tagged, pET28a (+) (EMD Biosciences, pET28a, Catalog #69864-3), pGEX-4T-1 (GST) vectors (Amersham, pGEX-4T-1, Catalog #27-4580-01). The point-mutation constructs including OTUD3 G288D were generated with a site-directed mutagenesis Kit (Stratagene, 200521). Introduction of the expression construct or siRNA/shRNA transfection was performed with Lipofectamine 3000 (Invitrogen, L3000-015) or Polyethylenimine-PEI or TransIntro EL Transfection Reagent (Transgen, FT201) according to the manufacturer's protocol. Adenovirus expressing PPAR $\delta$  and OTUD3 gene and vector control were from Vigene Biosciences (Jinan, China).

Medium with different glucose concentrations were prepared with DMEM without glucose (11966025, invitrogen) supplemented with glucose to indicated concentrations. Medium with different fatty acid concentrations were prepared with DMEM supplemented with equal molar amounts of oleic acid (Sigma) or palmitate (Sigma) with fatty-acid free BSA (Sigma) to total concentrations as indicated (Itani et al., 2000). For the half-life assay, cells were treated with the protein synthesis inhibitor CHX for indicated lengths of time before collection.

## METHOD DETAILS

### Whole exome sequencing

The procedure includes library preparation and sequencing, reads mapping to reference sequence, variant calling, functional annotation and filter. Details of extended protocols and the data analysis procedure are provided by Novogene (Beijing, China).

### Lentivirus packaging and infection (pCDH-CMV-MCS-EF1-Puro lentiviral system)

The pCDH-CMV-MCS-EF1-Puro lentiviral system (System Biosciences, pCDH-CMV-MCS-EF1-Puro) was used for OTUD3 WT and OTUD3 G288D overexpression vector. OTUD3 WT and OTUD3 G288D were cloned into the pCDH-CMV-MCS-EF1-Puro plasmid. pCDH, pCDH-OTUD3 WT, pCDH-OTUD3 G288D, pAX.2 (Addgene, psPAX2), and pMD.2G were co-transfected into HEK293T cells at a ratio of 4:3:1 for 36 hours, and cell culture media were collected. Next, the virus supernatant with polybrene (8  $\mu$ g/ml) was added into the culture medium for 24 hours to infect the target cells. Puromycin (2  $\mu$ g/ml) was used for sorting and selecting pCDH, pCDH-OTUD3 WT, pCDH-OTUD3 G288D positive cells to establish stable OTUD3 overexpression cell line.

### Lentivirus packaging and infection (pLKO.1-TRC lentiviral shRNA system)

The pLKO.1-TRC lentiviral shRNA system (Addgene, pLKO.1-TRC.mKO2, Plasmid #85208) was used for *Otud3* knockdown. shRNA targeting sequence for mouse OTUD3: (#2: TCATCAAGACGGAGCAAATAA, #3: AGACCGTGGACTACATGATAA) and for human OTUD3: (#2: TTTGGAAATCAGGGCTTAAA, #3: CAGAGCTCTTGGTGATCAATT) were cloned into the pLKO.1 plasmid. pLKO.1, pAX.2, and pMD.2G were co-transfected into 3T3-L1 or HEK293T cells at a ratio of 4:3:1 for 36 hours, and cell culture media were collected. The virus supernatant with polybrene (8  $\mu$ g/ml) was added into the culture medium for 24 hours to infect the target cells. Puromycin (2  $\mu$ g/ml) was used for sorting and selecting shRNA positive cells.

### Lentivirus packaging and infection (lentiCRISPR v2 system) in OTUD3 knockout stable cell line of HEK293T and 3T3-L1

The sequence (GCAAGCGGCGAAGAGCCGGCCGG) of the mouse *Otud3* gene (forward strand) in exon 1 was selected as the target. The sequence (CGGCGGAATCGGCCGAGTC) of the human *OTUD3* gene (forward strand) in exon 1 was selected as the target.

Oligos were purchased from Sangon and ligated into the lentiCRISPRv2 plasmid. The following lentivirus packaging and infection experimental protocol is similar to pLKO.1-TRC lentiviral shRNA system used in *Otud3* knockdown 3T3-L1 stable cell line.

### Intraperitoneal glucose and insulin tolerance tests

The intraperitoneal glucose tolerance test (GTT) was performed by intraperitoneal injection of D-glucose (2g/kg body weight) under fasting conditions for 12 hours. The insulin tolerance test (ITT) was performed by injecting mice intraperitoneally with insulin (0.4U/kg, Humulin-N from Eli Lilly or 0.8U/kg, Regular insulin, Wanbang) as indicated and diluted in 0.9% NaCl. Blood was collected from tail bleeds every 15 minutes over a 1.5-2 hours period, and blood glucose levels were measured using ACCU-CHEK performa (Roche Diagnostics).

### Serum insulin and lipid measurements

Mice were fasted for 12 hours prior to collecting blood. Serum was analyzed using the Insulin Mouse Ultrasensitive ELISA kit (cat# 80-INSMSU-E01, ALPCO), the Mouse Free and total cholesterol ELISA kit (cat# E1005, E1006, Applygen), WAKO 294-63601 and 290-63701 LabAssay Triglyceride assay kit were used to measure serum NEFA and triglyceride.

### PPAR $\delta$ agonist GW501516 treatment

Stock solutions of GW501516 (Enzo Life Sciences, Ann Arbor, MI) were prepared in ethyl alcohol. Fresh solution was diluted in PBS for intraperitoneal injection with a dose of 5mg/kg/day. 10 weeks' old *Otud3*<sup>-/-</sup> and wild-type male mice fed HFD were treated with GW501516 or same volume of vehicle for 7 weeks.

### Immunohistochemistry

Tissues were fixed in 10% formalin, dehydrated, embedded in paraffin, and sectioned for hematoxylin and eosin (H&E) staining. Images were captured using the Axio Vision 2.05 imaging system (Zeiss) and processed with Adobe Photoshop.

### Oil Red O Staining

Frozen sections of tissue from wild-type and *Otud3*<sup>-/-</sup> mice were fixed with 10% formalin. Oil Red O (Sigma-Aldrich) staining was performed using 60% isopropanol saturated with Oil Red O dye for 15min at 65°C.

### ATP content

Cellular and tissue ATP contents were measured using the ATP Bioluminescence Assay Kit HS II (Roche) in freshly prepared whole-cell or tissue lysates. Equal quantity of lysates was homogenized using a glass homogenizer. ATP content was measured on a 96-well plate (sterile, black) (Corning, Costar, catalog number: 3916).

### Mitochondria Isolation

Mitochondria were isolated from *Otud3*<sup>-/-</sup> mice and *Otud3*<sup>+/+</sup> tissues. Tissues were harvested, homogenized in mannitol/sucrose-ethylene glycol tetra-acetic acid (EGTA) buffer (225 mmol/L mannitol, 75 mmol/L sucrose, 5 mmol/L HEPES, and 1 mmol/L EGTA, pH 7.4) and was centrifuged at 800 x g for 5 min. The supernatant containing the cytoplasmic and mitochondrial fractions were transferred to a fresh tube and centrifuged for 5 min at 12,000 x g. Finally, mitochondria pellets were lysed with cell lytic MT (Sigma) containing protease and phosphatase inhibitors.

### Mitochondrial Electron Transport Chain Complex Activity Assays

Isolated mitochondria were used to measure mitochondrial electron transport chain complex activities. Complex I-V activities were determined by microplate assay kits (complex I: BC0510, Solarbio; complex II: BC3230, Solarbio; complex III: BC3245, Solarbio; complex IV: BC0945, Solarbio and complex V: BC1445, Solarbio) followed the manufacturer's instructions using UV7600 UV-Visible spectrophotometer (Lengguang Technology, China).

### Blue native PAGE (BN-PAGE) and blotting

Blue native (BN) PAGE and blotting was performed basically as described elsewhere (Konvalova, 2019) using polyacrylamide gradient gel. Briefly, mitochondrial pellets were resuspended in a mitochondrial buffer (1.75 M aminocaproic acid, 75 mM Bis-tris, 2 mM EDTA) then added fresh prepared 10% lauryl maltoside to the final concentration of 1%. After centrifuge at 20,000 x g for 20 min at 4 °C, the supernatants were collected and the protein concentrations were measured. A volume of sample buffer (containing 5% Coomassie blue G 250, 750 mM aminocaproic acid) that is half of the volume of lauryl maltoside were added. Equal amounts of mitochondria lysates loaded in a polyacrylamide gradient gel (3-13%) with blue cathode buffer (0.02% Coomassie blue G, 15 mM Bis-tris, 50 nM tricine) and anode buffer (50 mM Bis-tris). Samples were run at 40V for 15 min then 80V until the dye reaches 2/3 of the gel length. The blue cathode buffer was replaced with cathode buffer without Coomassie blue G and continue electrophoresis until the dye front has run out. The gel was rinsed in water and proteins were then transferred to the PVDF membrane by semi-dry blotting (constant voltage of 25 V for 30 min). Primary antibodies against OXPHOS complexes were anti-NDUFB8 antibody (complex I), anti-SDHA antibody (complex II), anti-UQCRC2 antibody (complex III), anti-COX4 antibody (complex IV) and anti-ATP5A antibody (complex V).

### Lactate measurement

Lactate was measured using an L-lactate assay kit (MAK065, Sigma). Equal amounts of cells were homogenized and the supernatant was colorimetrically determined by an absorbance measurement at 450 nm.

### Glucose uptake assay

Cells were washed twice with Krebs-Ringer-Phosphate-HEPES (KRPH) buffer and starved for glucose by incubation with KRPH buffer containing 0.2% bovine serum albumin (BSA) without glucose at 37 °C for 40 min. Glucose transport was determined by subsequent stimulation with 2-deoxy-D-glucose-6-phosphate (2DG6P) at a final concentration of 0.1 mM for 20 min. The reaction was stopped by washing the cells 4 times with ice-cold phosphate-buffered saline (PBS). The cells were lysed in lysis buffer, and glucose uptake was assessed using the Glucose Uptake Colorimetric assay kit (MAK083, Sigma) in accordance with the manufacturer's instructions. The absorbance was measured at a 412 nm wavelength on a microplate reader.

### Targeted metabolomics quantification by LC-MS

Targeted metabolomics quantification was carried out in our laboratory as described (Liu et al., 2017; Zhou and Yin, 2016). Briefly, TCA metabolites (citrate, succinate, fumaric acid, acetyl-CoA and succinyl-CoA) was measured from *Otud3<sup>+/+</sup>* and *Otud3<sup>-/-</sup>* mouse tissue lysates or plasma. Homogenized tissue or plasma mixed with 80% methanol and internal standard in methanol. Protein in the samples was precipitated by vortexing for 1 min, and supernatant was recovered following centrifugation at 12,000 rpm at 4 °C for 15 min. The supernatant was injected for LC-MS/MS analysis. The analyte and internal standard were separated on a Shimadzu Shim-pack XR-ODS column (4.6 × 50 mm, 2.2 μm) using 0.1% formic acid-water-methanol as mobile phase, with a runtime of 5 min. Detection was performed using negative ion electrospray tandem mass spectrometry via multiple reaction monitoring (MRM) scan mode furnished with analyst software workstation for data acquisition, qualitative and quantitative analysis.

### Measurement of oxygen consumption rate

Oxygen consumption rate (OCR) and extracellular acidification rate (ECAR) were measured using a Seahorse XF24 metabolic analyzer as indicated by the manufacturer (Seahorse XF Technology, Agilent). 3T3-L1 cells ( $2 \times 10^4$  cells per well) were seeded on XF24 plates (Agilent Seahorse). Cells were incubated for 50 min in a CO<sub>2</sub>-free incubator at 37 °C before loading the plate in the Seahorse analyzer. Oligomycin (2.5 μM), carbonyl cyanide-4-(trifluoromethoxy) phenylhydrazone (FCCP) (1.25 μM) and rotenone/antimycin A (1 μM each) were sequentially added to the cells and the OCR was monitored over time. The maximal respiratory capacity was calculated as the OCR after FCCP addition with subtraction of the OCR after oligomycin. For glycolysis (ECAR), cells were cultured in the absence of glucose and then XF media, glucose (10 mM), oligomycin (2.65 μM) and 2-deoxyglucose (100 mM) were sequentially added to the cells.

### Quantitative RT-PCR

Total RNA was freshly prepared using TRIzol (Invitrogen, 10296010). An aliquot of the total RNA was mixed with 0.5 μg random hexamer primer (Promega, A5000) in a 5 μL reaction volume. The mix were heated at 70 °C for 5 min and immediately chill for 5 min. RNAs was reverse-transcribed to cDNAs using GoScript Reverse Transcription System (Promega, A5000) at 25 °C for 5 min, 42 °C for 1 hour and 70 °C for 15 min in a 20 μL reaction volume followed the manufacturer's instruction. Quantitative RT-PCR was conducted with Qiagen QuantiNova SYBR green PCR Kit (Qiagen, 208054) on an ABI 7500 Real-Time PCR system (Applied Biosystems) using a hot-start SYBR-green-based method followed by melting curve analysis to verify specificity of the products. All reactions were run in duplicate with no template control. The qPCR conditions were: 95 °C for 5 min, followed by 45 cycles at 95 °C for 10 s, 60 °C for 10 s and 72 °C for 10 s. The Ct value (cycle number at threshold) was used to calculate the relative amount of mRNA. The Ct value of each determined RNA sample was normalized by subtracting that of control *Actin* or *Gapdh* RNA to obtain the ΔCt value, and the relative mRNA level was calculated as  $2^{-\Delta\Delta Ct}$ . Primer sets for quantitative RT-PCR were listed in Table 1.

### S-tag pulldown, Flag pulldown and Mass spectrometry analysis

Cell pellets or WAT were lysed with lysis buffer, incubated 4 hours with S-protein beads or overnight with Flag-beads and washed 3 times with lysis buffer. Flag pulldown and silver staining were performed according to manufacturers' instructions. Bands of interest were excised and subjected to liquid chromatography (LC)-MS/MS analysis (LTQ Orbitrap Elite).

### Confocal microscopy

For evaluation of GFP-OTUD3 localization under glucose and fatty acid stimuli, HeLa cells transfected with GFP-OTUD3 were seeded on glass cover slips in DMEM medium for 24 h. Cells were fixed with acetone for 10 min, followed by blocking with 1% BSA and staining with 0.5 μg/ml DAPI for 10 min at room temperature. Then the cover glasses were mounted and evaluated with fluorescence microscopy. A Nikon TCS A1 microscope was used for confocal microscopy.

### Co-immunoprecipitation assay (Co-IP)

Whole cellular extracts were prepared in RIPA buffer (50 mM Tris-HCl, pH 8.0, 150 mM NaCl, 1.5 mM MgCl<sub>2</sub>, 0.1% SDS, 0.5% Deoxycholate (DOC), 1% NP-40, 1 mM PMSF, 1 × protease inhibitor cocktail (Roche, 04693116001), 1 × Phosphatase Inhibitor cocktail (Roche, 04906837001), 1 μg/ml aprotinin, 1 μg/ml leupeptin, 1 μg/ml pepstatin). 2 μg of the indicated antibody (or 20 μl Flag M2

Affinity Gel (Sigma, A2220)) was added into whole cellular extracts and incubated overnight at 4 °C. After washing with RIPA buffer three times, the binding components were eluted using Flag peptide (Sigma, F3290), or by boiling with 2×SDS-PAGE loading buffer, and were analyzed with western blot.

### Chromatin-immunoprecipitation sequencing (ChIP-seq)

Mice were transfected with AAV2-Otud3-Flag according to a previous study (Huang et al., 2017), and the epididymal adipose tissues were removed at the 4<sup>th</sup> week after injection. The adipose tissues of 3 different mice were dissociated into single cells by collagenase and purified by centrifugation. One-step crosslinking ChIP experiment was performed using 1% formaldehyde for 10 min at RT. Chromatin was sheared with a Chip grade indirect sonication water baths of Qsonica Q700 Sonicator (Qsonica, USA) for 60 cycles (10s on/10s off). Then, sheared chromatin subjected to ChIP using ChIP-grade anti-Flag antibody to precipitate flag-tagged OTUD3 with the ChIP Assay Kit (17-371, Millipore) according to the manufacturer's instructions. Libraries were purified, quantified, multiplexed and submitted to 75 bp single-end sequencing using the NovaSeq 6000 sequencing system (Illumina). Details of extended protocols and the data analysis procedure are provided by Novogene (Beijing, China).

### Cytoplasmic and nuclear fractions preparation

Cells or mouse tissues were harvested, rinsed with PBS (137 mM NaCl, 2.7 mM KCl, 10 mM Na<sub>2</sub>HPO<sub>4</sub>, 1.8 mM KH<sub>2</sub>PO<sub>4</sub>) and pelleted. Cells or mouse tissue were then suspended or homogenized in 5 volumes of cold Buffer A (10 mM HEPES pH 7.9, 0.1 mM EDTA, 0.1 mM EGTA, 10 mM KCl, protease inhibitor cocktail (Roche), 1 mM DTT, 0.15% NP-40), and allowed to swell on ice for 15 min, the homogenate was spun for 2 min at 12,000 g. The supernatant containing the cytoplasm fraction was transferred to a fresh tube. The crude nuclear pellet was suspended in buffer B (10 mM Tris pH 7.9, 1.5 mM MgCl<sub>2</sub>, 10 mM KCl, 400 mM NaCl, 0.4% Triton X-100, protease inhibitor cocktail (Sigma), and vigorously vortexed at 4 °C for 30 min. The homogenate was centrifuged for 15 min at 12,000 g, and the nuclear extract was transferred to a fresh tube.

### RNA-seq procedures

Total RNA was isolated from sample using RNeasy mini kit (Qiagen, Germany). Paired-end libraries were synthesized by using the TruSeq RNA Sample Preparation Kit (Illumina, USA) following TruSeq RNA Sample Preparation Guide. The library was sequenced on the Illumina HiSeq X-ten platform (Illumina, USA). Details of extended protocols and the data analysis procedure are provided by SHBIO (Shanghai, China).

### OTUD3 protein purification

Human cDNA for OTUD3 were respectively cloned into a pGEX-4T-1 and pET28a (+) vector with a N-terminal GST-tag and purified from the Escherichia coli strain BL21 (Invitrogen) using GST Agarose beads and Ni-Agarose beads (Qiagen) separately.

### Ubiquitinated protein purification

To purify ubiquitinated protein, HEK293T cells were transfected with Flag-protein and HA-Ub. 48 hours later, cells were lysed with RIPA lysis buffer. The cell extracts were subjected to immunoprecipitation using anti-Flag M2 beads, followed by Flag peptide elution.

### Deubiquitination assay for ubiquitinated protein

For the cell free deubiquitination assay, purified protein-Ub protein was incubated with purified GST-OTUD3, GST-OTUD3 G288D protein in a 5×deubiquitination buffer (100 mM Tris-HCl, PH 7.4, 250 mM NaCl, 25 mM MgCl<sub>2</sub>, 5 mM 2-mecaptoenthanol, 50% glycerol) for 45 mins at 37 °C. The reaction mixtures were resolved on an 8% gel for Western blot analysis using anti-Flag or anti-HA antibody.

For intracellular deubiquitination assays, Cells were transfected with Flag-protein, His-HA-Ub or c-Myc-OTUD3. 48 hours later, cells were lysed with RIPA lysis buffer and were subjected to affinity purification with anti-Flag M2 beads. After washing with RIPA buffer three times, the binding components were eluted using Flag peptide (Sigma, F3290), or by boiling with 2×SDS-PAGE loading buffer, and were analyzed by western blot. Eluted proteins were resolved on an 8% gel for Western blot analysis.

### Metabolic cage

Mice were acclimated to single cage housing for a week into CLAMS metabolic cage (Columbus Instruments). O<sub>2</sub> consumption (VO<sub>2</sub>) and CO<sub>2</sub> expiration (VCO<sub>2</sub>) were measured for 1 min with 14 min intervals at a flow rate set to 0.72 l.p.m. Respiratory Exchange Ratio (RER) was calculated by dividing VCO<sub>2</sub>/VO<sub>2</sub>. Locomotor activity, food and water intake was measured simultaneously by built-in detection system. Sufficient foods (ND or HFD) and water were provided at the beginning of experiences, the chambers were then locked and researchers did not perform any additional manipulation during the whole experiences.

### QUANTIFICATION AND STATISTICAL ANALYSIS

Data are shown as mean ± SEM. Statistical analyses, unless otherwise indicated, were performed using GraphPad Prism 9. Statistical significance was calculated using two-tailed unpaired Student's t test when two independent groups were compared. For

multiple groups comparisons, two-way ANOVA was applied unless otherwise indicated. Post-hoc analysis was performed on the ANOVA using Holm-Sidak's multiple comparisons or by controlling the False Discovery Rate using the method of Benjamini, Krieger and Yekutieli as appropriate. p values below 0.05 were considered statistically significant. \*p < 0.05, \*\*p < 0.01 and \*\*\*p < 0.001. Differentially expressed genes of RNA-seq data were identified using edgeR. The significance threshold in multiple tests was set by the False Discovery Rate < 0.05. The statistical parameters for each experiment can also be found in the figure legends.